UNIVERSIDADE FEDERAL DE MINAS GERAIS
Instituto de Ciências Exatas
Programa de Pós-graduação em Física

Diego Leonardo Braga Ferreira

QUANTUM CORRELATIONS, ENTANGLEMENT SPECTRUM AND COHERENCE OF TWO-PARTICLE REDUCED DENSITY MATRIX IN THE EXTENDED HUBBARD MODEL

Belo Horizonte
2023

Diego Leonardo Braga Ferreira

QUANTUM CORRELATIONS, ENTANGLEMENT SPECTRUM AND COHERENCE OF TWO-PARTICLE REDUCED DENSITY MATRIX IN THE EXTENDED HUBBARD MODEL

Tese apresentada ao Programa de Pós-Graduação em Física do Instituto de Ciências Exatas da Universidade Federal de Minas Gerais como requisito parcial para obtenção do título de Doutor em Ciências.

Orientador: Reinaldo Oliveira Vianna
Coorientador: Fernando Iemini de Rezende Aguiar

Belo Horizonte
2023

Dados Internacionais de Catalogação na Publicação (CIP)

F383q Ferreira, Diego Leonardo Braga.
Quantum correlations, entanglement spectrum and coherence of two-particle reduced density matrix in the extended Hubbard model / Diego Leonardo Braga Ferreira. – 2023.
59 f. : il.

Orientador: Reinaldo Oliveira Vianna.
Coorientador: Fernando Iemini de Rezende Aguiar.
Tese (doutorado) – Universidade Federal de Minas Gerais, Departamento de Física.
Bibliografia: f. 46-59.

1. Modelo de Hubbard. 2. Matriz de densidade. 3. Transições de fases. I. Título. II. Vianna, Reinaldo Oliveira. III. Aguiar, Fernando Iemini de Rezende. IV. Universidade Federal de Minas Gerais, Departamento de Física.

CDU – 530.145.6 (043)

Ficha catalográfica elaborada por Romário Martins Ribeiro – CRB6 3595
Biblioteca Professor Manoel Lopes de Siqueira – Departamento de Física - UFMG

UNIVERSIDADE FEDERAL DE MINAS GERAIS
INSTITUTO DE CIÊNCIAS EXATAS
PROGRAMA DE PÓS-GRADUAÇÃO EM FÍSICA

ATA DE DEFESA DE TESE

ATA DA SESSÃO DE ARGUIÇÃO DA 411ª TESE DO PROGRAMA DE PÓS-GRADUAÇÃO EM FÍSICA, DEFENDIDA POR DIEGO LEONARDO BRAGA FERREIRA orientado pelo professor Reinaldo Oliveira Vianna e coorientado pelo professor Fernando Iemini de Rezende, para obtenção do grau de **DOUTOR EM CIÊNCIAS, área de concentração Física**. Às 9 horas de dois de fevereiro de dois mil e vinte e três reuniu-se, por videoconferência, a Comissão Examinadora, composta pelos professores **Reinaldo Oliveira Vianna** (Orientador - Departamento de Física/UFMG), **Fernando Iemini de Rezende** (Coorientador - Instituto de Física/UFF), **Leonardo Teixeira Neves** (Departamento de Física/UFMG), **Walber Hugo de Brito** (Departamento de Física/UFMG), **Eduardo Inácio Duzzioni** (Departamento de Física/UFSC) e **Vivian Vanessa França Henn** (Instituto de Química/UNESP) para dar cumprimento ao Artigo 37 do Regimento Geral da UFMG, submetendo o Mestre **DIEGO LEONARDO BRAGA FERREIRA** à arguição de seu trabalho de Tese de Doutorado, que recebeu o título de "**Quantum correlations, entanglement spectrum and coherence of two-particle reduced density matrix in the Extended Hubbard Model"**. O candidato fez uma exposição oral de seu trabalho durante aproximadamente 50 minutos. Após esta, os membros da comissão prosseguiram com a sua arguição, e apresentaram seus pareceres individuais sobre o trabalho, concluindo pela aprovação do candidato.

Belo Horizonte, 02 de fevereiro de 2023.

Prof. Reinaldo Oliveira Vianna	Prof. Walber Hugo de Brito
Orientador do estudante	Departamento de Física/UFMG
Departamento de Física/UFMG	
Prof. Fernando Iemini de Rezende	Prof. Eduardo Inácio Duzzioni
Coorientador do estudante	Departamento de Física/UFSC
Instituto de Física/UFF	
Prof. Leonardo Teixeira Neves	Prof. Vivian Vanessa França Henn
Departamento de Física/UFMG	Instituto de Química/UNESP

Candidato: Diego Leonardo Braga Ferreira

Documento assinado eletronicamente por **Reinaldo Oliveira Vianna**, **Professor do Magistério Superior**, em 02/02/2023, às 15:41, conforme horário oficial de Brasília, com fundamento no art. 5º do Decreto nº 10.543, de 13 de novembro de 2020.

Documento assinado eletronicamente por **Vivian Vanessa França Henn**, **Usuária Externa**, em 02/02/2023, às 15:50, conforme horário oficial de Brasília, com fundamento no art. 5º do Decreto nº 10.543, de 13 de novembro de 2020.

Documento assinado eletronicamente por **Leonardo Teixeira Neves**, **Professor do Magistério Superior**, em 02/02/2023, às 16:14, conforme horário oficial de Brasília, com fundamento no art. 5º do Decreto nº 10.543, de 13 de novembro de 2020.

Documento assinado eletronicamente por **Eduardo Inacio Duzzioni**, **Usuário Externo**, em 02/02/2023, às 16:25, conforme horário oficial de Brasília, com fundamento no art. 5º do Decreto nº 10.543, de 13 de novembro de 2020.

Documento assinado eletronicamente por **Walber Hugo de Brito**, **Professor do Magistério Superior**, em 02/02/2023, às 16:47, conforme horário oficial de Brasília, com fundamento no art. 5º do Decreto nº 10.543, de 13 de novembro de 2020.

Documento assinado eletronicamente por **Fernando Iemini de Rezende Aguiar**, **Usuário Externo**, em 02/02/2023, às 17:09, conforme horário oficial de Brasília, com fundamento no art. 5º do Decreto nº 10.543, de 13 de novembro de 2020.

Documento assinado eletronicamente por **Diego Leonardo Braga Ferreira**, **Usuário Externo**, em 07/02/2023, às 10:27, conforme horário oficial de Brasília, com fundamento no art. 5º do Decreto nº 10.543, de 13 de novembro de 2020.

A autenticidade deste documento pode ser conferida no site https://sei.ufmg.br/sei/controlador_externo.php?acao=documento_conferir&id_orgao_acesso_externo=0, informando o código verificador **2059474** e o código CRC **077FE33B**.

Dedico esta tese primeiramente ao meu Senhor e Salvador Jesus Cristo, Filho de Deus, que dá a este empreendimento um motivo e razão. Sem ele, nada teria sentido. Obrigado por sustentar meu ser, por me amar tanto e ser tão misericordioso.

Dedico também ao meu pai Nélio, pois sem seu incentivo, carinho e exemplo não teria chegado onde cheguei. Que minha defesa honre todo esforço depositado em mim, muito obrigado por ter sido o melhor pai do mundo. Nos encontramos em breve.

Dedico esta tese a minha mãe Bete, que também sempre esteve comigo nos momentos mais difíceis, me apoiando com seu cuidado e amor.

Dedico a minha irmã Diana e a minha sobrinha Sofia, que amo infinitamente e que me proporcionaram sorrisos e alegrias nos momentos mais difíceis que passei na minha vida durante o doutorado.

Agradeço a todos os meus familiares, dentre eles meu tio Somsom, que talvez tenha sido a pessoa que mais me influenciou a ser cientista. Ainda lembro das nossas conversas sobre o universo em cima da árvore quando ainda era criança, e do fascínio que tinha por estes assuntos.

Dedico também à minha namorada e amiga de infância Jamile, que tanto me entendeu e apoiou nesta tarefa que parecia não ter fim.

Dedico ao meu orientador Reinaldo, por todas as discussões, conhecimento passado, conversas em botecos e pela compreensão quando mais precisei. Muito obrigado amigo.

Dedico ao meu co-orientador Iemini, pelas discussões e ânimo no desenvolvimento do artigo. Posso dizer sem dúvidas que se não fosse pelo seu entusiasmo e ajuda não teria chegado aqui, amigo.

Dedico a todos os meus amigos, dentro e fora da UFMG, que de alguma forma contribuiram e ajudaram no desenvolvimento da tese e pessoal, laços que quero manter pra vida inteira.

Dedico ao meu psiquiatra e xará Diego, pelo seu excelente trabalho em me fazer enxergar cores de novo e terminar meu doutorado.

Dedico também à população brasileira que financiou este trabalho com suor sagrado. Este tese pertence a todos vocês.

Agradecimentos

Agradeço pelo suporte financeiro das agências de fomento brasileiras FAPEMIG (Fundação de Amparo à Pesquisa do Estado de Minas Gerais), CAPES (Coordenação de Aperfeiçoamento de Pessoal de Nível Superior), CNPq (Conselho Nacional de Desenvolvimento Científico e Tecnológico) e INCT-IQ (National Institute of Science and Technology for Quantum Information). Fernando Iemini agradece às agências CNPq (Grant No. 308205/2019-7) e FAPERJ (Grant No. E-26/211.318/2019). Agradeço também à biblioteca ITensor [1, 2] que nos forneceu a funcionalidade básica para o desenvolvimento do nosso código que está disponível em um repositório público [3] e pode ser usado livremente de acordo com sua licença.

"Menos é mais."

Ludwig Mies van der Rohe

Resumo

Estudamos as propriedades do estado fundamental do modelo de Hubbard estendido unidimensional com meio preenchimento de elétrons da perspectiva de sua matriz densidade reduzida de *partícula*. Focamos na matriz de densidade reduzida de 2 férmions e realizamos uma análise de suas correlações quânticas e coerência ao longo das diferentes fases do modelo. Especificamente, estudamos sua (i) entropia de emaranhamento, (ii) norma de coerência ℓ_1, (iii) matriz de cumulante irredutível de dois corpos e (iv) espectro de emaranhamento. Nossos resultados mostram que essas diferentes propriedades se complementam dependendo da fase do sistema, exibindo comportamentos peculiares como descontinuidades, valores máximos ou mínimos nas transições quânticas de fase, proporcionando assim uma visão qualitativa do diagrama de fases do modelo. Em particular, na região supercondutora, obtemos que o espectro de emaranhamento sinaliza uma transição no sistema entre ordenamentos de emparelhamento dominante do tipo singleto (SS) para tripleto (TS). Além disso, a partir da análise do autovetor dominante no estado reduzido, podemos relacionar a transição SS-TS com a separação espacial entre os pares de férmions nos dois diferentes ordenamentos de pareamento.

Palavras-chave: Modelo de Hubbard Estendido. Matriz de Densidade Reduzida. Correlações Quânticas. Coerência. Transições de Fase Quânticas. Espectro de Emaranhamento. Transição entre Fases Supercondutoras do tipo Singleto e Tripleto.

Abstract

We study the ground state properties of the one-dimensional extended Hubbard model at half-filling from the perspective of its *particle* reduced density matrix. We focus on the reduced density matrix of 2 fermions and perform an analysis of its quantum correlations and coherence across the different phases of the model. Specifically, we investigate its (i) entanglement entropy, (ii) ℓ_1 norm of coherence, (iii) irreducible two-body cumulant matrix, and (iv) entanglement spectrum. Our results show that these different properties are complementary, depending on the phase of the system, exhibiting peculiar behaviors such as discontinuities or maximum/minimum values at the quantum phase transitions, which provides a qualitative view of the phase diagram of the model. In particular, in the superconducting region, we obtain that the entanglement spectrum signals a transition between a dominant singlet (SS) and triplet (TS) pairing ordering in the system. Moreover, from the analysis of the dominant eigenvector in the reduced state, we can relate the SS-TS transition to the spatial separation between the fermion pairs in the two different pairing orderings.

Keywords: Extended Hubbard Model. Reduced Density Matrix. Quantum Correlations. Coherence. Quantum Phase Transitions. Entanglement Spectrum. Singlet and Triplet Superconducting Phase Transition.

Sumário

1 Introduction

1.1 Motivation

A wide range of condensed matter phases can emerge when the constituents of the system are brought together and allowed to interact with each other. Due to the many-body interactions among its constituents, when the number of constituents is large, the system condenses into a collective behavior with specific macroscopic properties [4]. Most familiar examples of condensed matter phases include magnetism, arising from the exchange interaction between local magnetic moments; solids and liquids, which arise from the electromagnetic forces between atoms; superconductors or superfluids, arising from the interaction between fermions or bosons; as well as more unconventional ones such as topological phases, emerging from nonlocal correlations among its constituents [5].

There are different ways of analysing many-body phases. In conventional phases, one can usually rely on the structure of the system's local correlations and corresponding order parameters, which provide information about the macroscopic properties of the system. In recent years, different approaches have also been put forward, relying on interesting connections between Quantum Information and Condensed Matter theories. Much activity has been conducted on the border of these fields and many interesting concepts have been addressed [6]. In particular, quantum information insights about many-body entanglement have proved a powerful tool in the study and characterization of many-body systems, giving a unique perspective in our understanding of condensed matter phases [7].

The entanglement between the constituents of the system is shown to be tightly connected to the characteristics of the different phases that a model can support. When the system is driven along a quantum phase transition, entanglement can often show peculiar critical behaviors, offering a qualitative display of the transition and a deeper characterization of the many-body wavefunction [6]. However, quantum correlations and many-body entanglement of a system can appear in different forms among its constituents, and it is usually a very hard task to highlight all its different intricate structures and to quantify them properly.

The usual approach deals with the entanglement between two partitions of the system, which, for a pure global state, can be easily quantified by the von Neumann entropy of the reduced density matrix. More recently it was realized that not only the von Neumann entropy of the reduced density matrix has important information about the phase, but also its spectral properties, i.e., the eigenvalues of the reduced density matrix - usually called as entanglement spectrum - can host valuable and more detailed

information about the phase [8–10]. As for example, in unconventional topological phases in which the entanglement spectrum becomes degenerate due to the presence of non abelian edge excitations in the system. Apart from bipartite entanglement, different quantum correlations and entanglement quantifiers were also put forward [6, 11–13], including for example the analysis of total correlations [14], multipartite entanglement [6,15–17], pairwise concurrences and quantum discord quantifiers [11, 18–22], particle entanglement [23–31], coherences [13, 32] among others [33]. In a general form, these studies proved very fruitful highlighting how different facets of the correlations shared between the microscopic constituents can be useful and complementary to each other for a complete characterization of quantum systems and their phases of matter. We shall explore one of these facets in this thesis, specifically, the *particle correlations* shared among its constituents.

In this thesis, we thus study the one-dimensional extended Hubbard model (EHM) [34] within the perspective of its *n-particle reduced density matrices* (n-particle RDM). The core work and results presented in this thesis have been published in the following article: [35]. Specifically, we focus on the $n = 2$ case, corresponding to the two-body reduced density matrices. We analyse the quantum correlations and many-body entanglement present in the reduced density matrices among the different phases of the model and across its quantum phase transitions. Most studies of the EHM in the quantum information context have dealt with the quantum correlations and entanglement among the *modes* of the system [36–45]. Here modes can be any defined set of single particle degrees of freedom, as e.g., the spatial localized degrees along the sites of the chain, or (spatially delocalized) momentum degrees of freedom for single particles. It was first observed by Shi-Jian Gu et al. [36] that the entanglement of a single site with the rest of the chain is sensitive to three main symmetry broken phases of the model, namely the charge-density-wave (CDW), spin-density wave (SDW) and phase separation (PS). Further investigation considering the entanglement of spatial blocks with ℓ sites and the rest of the chain [37] showed to be even more sensitive to other phases, as superconducting and bond ordered phases. In a previous work [23], we started our investigations within this different perspective, i.e., analysing the quantum correlation of the particle reduced density matrix. Our results focused in the case of $n = 1$, showing that the von Neumann entropy of the 1-particle RDM (usually called as entanglement of particles or fermionic entanglement [46–67]) is useful for the analysis of the model, capturing its main phase transitions except for subtle transitions between different superconducting forms, and the bond-order wave phase. Therefore, in this work we take a step beyond the simplest $n = 1$ case, considering the more general case with $n = 2$, which contains further information about the correlations and properties of the system [68]. We perform a thorough analysis of the RDM properties using different quantum information and many-body quantum correlation tools. Specifically, we analyse not only its (i) von Neumann entropy, quantifying the entanglement of these particles with the rest of the system; as well as its (ii) quantum coherence, as a direct manifestation of

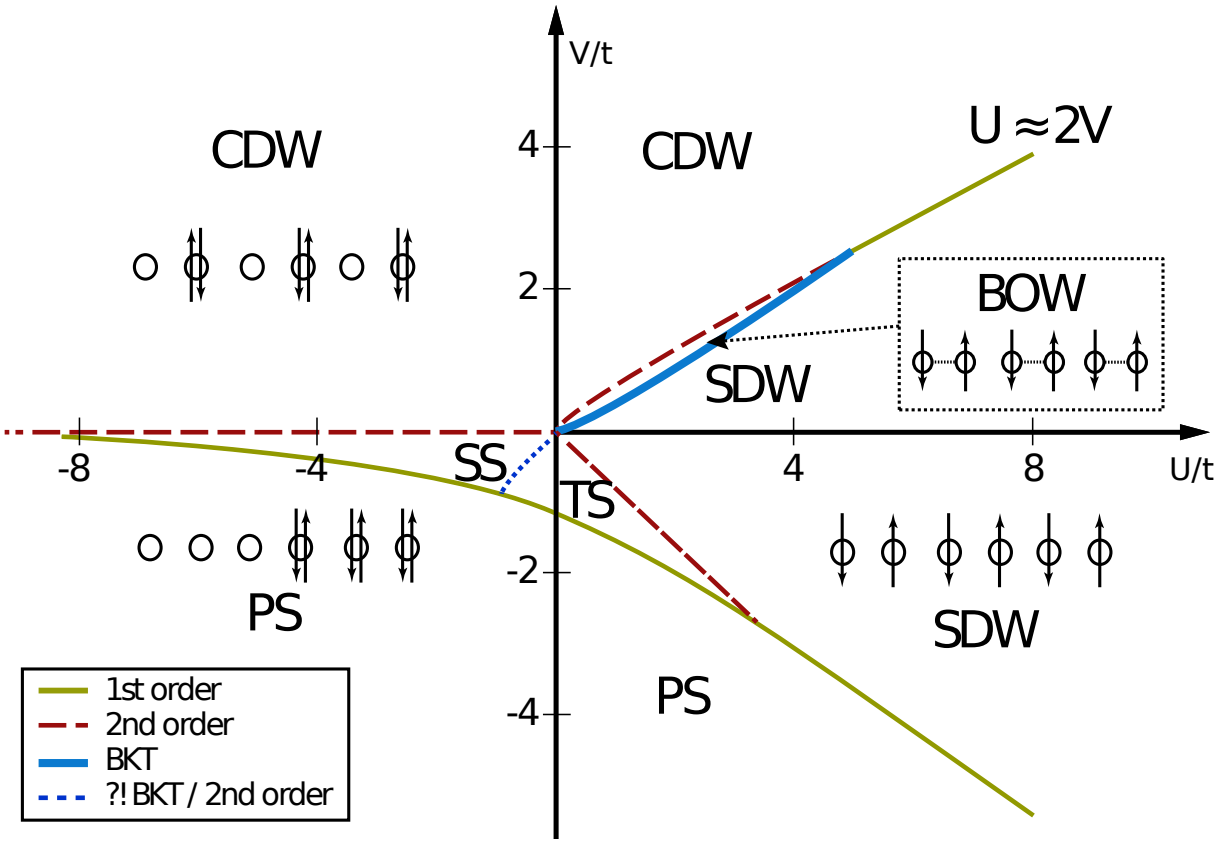

Figure 1 – Schematic picture for the phase-diagram of the model, highlighting its different phases and quantum phases transitions as discussed in the literature (see main text).

the quantum superposition principle in the reduced states; (iii) entanglement spectrum and entanglement gap, providing a more detailed information of the spectrum structure on the different phases; and (iv) its 2-body cumulant, which is a genuinely two-body correlation matrix, i.e., cannot be described from its 1-particle RDM. In a general form, we obtained that these quantifiers are sensitive to most phases of the model, showing peculiar behavior at their quantum phase transitions. Depending on the specific phase or quantum phase transitions under scrutiny, the analysis of these quantifiers can be complementary, providing different facets of the quantum system (*e.g.* different forms of superconductivity in the model are not easily perceived from quantifiers (i)-(ii)-(iii)-nor from its simpler 1-particle RDM- while the entanglement spectrum can discriminate it).

1.2 Extended Hubbard Model

In this section we review the main properties of the one-dimensional extended Hubbard model. All of our studies are focused in the half-filling case. The reader familiar with the model might skip to the next section.

The EHM model is a generalisation of the usual Hubbard model [34, 69], encompas-

sing broader interactions between the fermionic particles, such as an inter-site interaction, thus supporting a richer phase diagram. Precisely, the model is described as,

$$\begin{aligned} H_{EHM} &= -t\sum_{j=1}^{L}\sum_{\sigma=\uparrow,\downarrow}(\hat{a}^{\dagger}_{j,\sigma}\hat{a}_{j+1,\sigma}+\hat{a}^{\dagger}_{j+1,\sigma}\hat{a}_{j,\sigma})+ \\ &\quad +U\sum_{j=1}^{L}\hat{n}_{j\uparrow}\hat{n}_{j\downarrow}+V\sum_{j=1}^{L}\hat{n}_{j}\hat{n}_{j+1}, \end{aligned} \tag{1.1}$$

where L is the lattice size, $\hat{a}^{\dagger}_{j,\sigma}$ and $\hat{a}_{j,\sigma}$ are creation and annihilation operators, respectively, of a fermion with spin $\sigma =\uparrow,\downarrow$ at site j, $\hat{n}_{j,\sigma}=\hat{a}^{\dagger}_{j,\sigma}\hat{a}_{j,\sigma}$, $\hat{n}_j=\hat{n}_{j,\uparrow}+\hat{n}_{j,\downarrow}$. The hopping (tunnelling) between neighbor sites is parametrized by t, while the on-site and inter-site interactions are given by U and V, respectively. We set $t=1$ as defining our energy scale.

Many efforts have been devoted to the investigation of the phase diagram of the EHM at half filling, with methods ranging from analytical, perturbative, approximations based on bosonization as well as numerical ones [70–80]. Despite the apparent simplicity of the model it is predicted to exhibit a very rich phase diagram. The model can support several distinct phases, namely: spin-density wave (SDW), singlet (SS) and triplet (TS) superconductors, phase separation (PS), charge-density wave (CDW) and bond-order wave (BOW) - see Fig.(1) for a sketch of the phase diagram.

In the strong coupling limits, it is intuitive the characterization of the different phases the model can support. In the case of strong repulsive onsite interaction, $U>0$, $U\gg V$, the fermions avoid double occupation and due to the hopping an antiferromagnetic ordering between neighbor sites is formed, generating a periodic modulation of spins along the chain, so-called spin density wave (SDW). The presence of such a phase can be captured by the analysis of the ground state spin correlations $\langle\sigma^z_j\sigma^z_\ell\rangle$, which exhibit a staggered (alternating) pattern, where $\sigma^z_j=\frac{1}{2}(\hat{n}_{j\uparrow}-\hat{n}_{j\downarrow})$.

In the opposite case of a strong repulsive inter-site interaction, $V>0$, $V\gg U$, particles avoid occupying neighbor sites, tending in this way to occupy the same sites. A periodic modulation of charge is now formed, creating a charge-density wave pattern captured by density-density correlations $\langle\hat{n}_j\hat{n}_\ell\rangle$, which exhibit an alternating (staggered) pattern, in the ground state wavefunction.

In the case of strong attractive interactions ($U,V<0$ or $U>0$, $V<0$ with $|V|\gg|U|$), the particles tend to cluster together and the ground state becomes inhomogeneous with different average charge densities in distinct spatial regions. Such a phase is called phase separation (PS) and can be observed from the analysis of the charge profile along the chain, which shows a non-uniform distribution with distinct regions of high and low density.

In the weak coupling limit the analysis becomes subtler, since perturbative arguments might not be accurate and intuition might fail. For small attractive inter-site

interactions ($V < 0$), superconducting phases are expected to appear, characterized by the pairing of fermions which could be observed from pairing correlations. The fermions can be paired in different forms, with the possibility of singlet or triplet pairings to occur. It is predicted [70, 71] a singlet-superconductor (SS) for approximately $U \leq 2V$, while a triplet-superconducting (TS) for $U \geq 2V$.

The last phase in the model is the controversial bond-order-wave (BOW). For small to intermediate values of positive U and V, in a narrow strip between CDW and SDW phases, it has been predicted [71–77] the appearance of a phase exhibiting alternating strengths for the expectation value of the kinetic energy operator on the bonds, characterized by the order parameter $\langle \hat{B}_{j,j+1} \hat{B}_{\ell,\ell+1} \rangle$, where $\hat{B}_{m,m+1} = \sum_\sigma (\hat{a}^\dagger_{m,\sigma} \hat{a}_{m+1,\sigma} + H.c.)$ is the kinetic energy operator associated with the m'th bond. Such a phase should appear from (i) a continuous CDW-BOW transition; and (ii) a Berezinskii-Kosterlitz-Thouless (BKT) transition from BOW to SDW. While from one side the CDW-BOW phase boundary can be well resolved, described by a standard second order phase transition, the BOW-SDW boundary is more difficult to locate it precisely, since it involves a BKT transition, a topological transition of infinite order that is not characterized by a local order parameter. The BKT transition line remains a challenge to delineate and is still subject to debate [72–74, 76, 77].

1.3 Organization

The thesis is organized as follows. In Chap. 2 we review the definition of n-particle reduced density matrices and their properties. We also introduce the quantum correlation and entanglement quantifiers studied in this thesis, as well as the concept of entanglement spectrum and entanglement gap. In Chap. 3 we review the numerical techniques based on Matrix Product States (MPS) used to obtain ground states and correlation functions. In Chap. 4 we present our results. We first discuss the general qualitative behavior of the quantifiers in the whole phase diagram and then perform a deeper analysis of finite-size scalings and spectral properties along specific regions in the model.

We also emphasize that this thesis is not an extensive and complete material on the subject addressed, but it intends to be a direct and humble exposition of several extensive subjects, always bringing references to the readers.

2 Review: Reduced Density Matrices of Indistinguishable Particles

2.1 n-Particle Reduced Density Matrix

In this section we review the definition and some properties of particle reduced density matrices. In a system of N indistinguishable fermions, described by the set of anticommuting creation (and annihilation) operators $\{\hat{a}^\dagger_{i,\sigma}\}$ ($\{\hat{a}_{i,\sigma}\}$), where $i = 1, ..., L$ stands for the site index and $\sigma =\uparrow,\downarrow$ for the spin index, a pure state can always be expanded in the following form,

$$|\psi\rangle = \sum_{i_1 \ldots i_N=1}^{L} \sum_{\sigma_1 \ldots \sigma_N=\uparrow,\downarrow} \omega_{i_1\sigma_1 \ldots i_N\sigma_1}\ \hat{a}^\dagger_{i_1,\sigma_1} \ldots \hat{a}^\dagger_{i_N,\sigma_N} |vac\rangle\,, \tag{2.1}$$

where the coefficients $\omega_{i_1\sigma_1 \ldots i_N\sigma_N}$ are antisymmetric in all indices, satisfy the normalization condition of the state and $|vac\rangle$ is the vacuum state. We can compute the n-particle reduced density matrix $\hat{\rho}_n$ ($1 \leq n \leq N-1$) of n fermions performing the partial trace over the rest $N-n$ fermions, as follows,

$$\hat{\rho}_n = Tr_{(n+1,\ldots,N)} \left(|\psi\rangle \langle\psi|\right). \tag{2.2}$$

The partial trace defines a bipartition $n : N-n$ between n fermions and the rest of the system. Usually the calculation of the particle reduced density matrix using the partial trace described above can be cumbersome. We can, however, obtain it in a different way, which will turn useful for our purposes. Instead of taking the partial trace one can compute all n-body correlators, which correspond to the matrix elements of $\hat{\rho}_n$, and in this way reconstruct the reduced state as in a tomographic process. In other words, the reduced density matrices of one and two fermions have the following entries:

$$[\hat{\rho}_1]_{(i\sigma_i),(j\sigma_j)} = \binom{N}{1}^{-1} \langle\psi|\, \hat{a}^\dagger_{i\sigma_i} \hat{a}_{j\sigma_j} |\psi\rangle\,, \tag{2.3}$$

$$[\hat{\rho}_2]_{(i\sigma_i j\sigma_j),(k\sigma_k \ell\sigma_\ell)} = \binom{N}{2}^{-1} \langle\psi|\, \hat{a}^\dagger_{i\sigma_i} \hat{a}^\dagger_{j\sigma_j} \hat{a}_{k\sigma_k} \hat{a}_{\ell\sigma_\ell} |\psi\rangle\,, \tag{2.4}$$

where $\binom{N}{M}$ is the binomial coefficient. One can also obtain the 1-particle reduced density matrix from an integration of the 2-particle reduced density matrix,

$$[\hat{\rho}_1]_{(i\sigma_i),(j\sigma_j)} = \mathcal{N} \sum_{k,\sigma_k} [\hat{\rho}_2]_{(i\sigma_i k\sigma_k),(k\sigma_k j\sigma_j)} \tag{2.5}$$

with $\mathcal{N} = 1/2$ the normalization constant. In general, an n-particle RDM can always be obtained from its higher orders ($k > n$)-particle RDM from a proper integration over its

tensor elements. The inverse is obviously not true. It is important to recall, however, that the elements of higher orders ($k > n$)-particle RDM are partially related to the elements of their lower orders, apart from their cumulants [81]. Specifically, for the case of 2-particle RDM, its elements are formally decomposed into a reducible part, built from the 1-particle RDM, and an irreducible part, which is *defined* as the two-particle cumulant $\hat{\Delta}_2$:

$$\binom{N}{2}\left[\hat{\rho}_2\right]_{(i\sigma_i j\sigma_j),(k\sigma_k\ell\sigma_\ell)} = N^2\left[\hat{\rho}_1\right]_{(i\sigma_i),(k\sigma_k)}\left[\hat{\rho}_1\right]_{(j\sigma_j),(\ell\sigma_\ell)} - N^2\left[\hat{\rho}_1\right]_{(i\sigma_i),(\ell\sigma_\ell)}\left[\hat{\rho}_1\right]_{(j\sigma_j),(k\sigma_k)} + \left[\hat{\Delta}_2\right]_{(i\sigma_i j\sigma_j),(k\sigma_k\ell\sigma_\ell)} \tag{2.6}$$

where $\hat{\Delta}_2$ is the 2'nd order cumulant, corresponding to the elements of $\hat{\rho}_2$ that cannot be obtained from lower orders $\rho_{n<2}$. We can see that cumulants are Hermitian matrices. This follows from Eq. (2.6), as the cumulant is the difference between two Hermitian matrices: $\hat{\rho}_2$ (which is Hermitian by definition as a density matrix) and the reducible part (the terms constructed from $\hat{\rho}_1$), which is also Hermitian.

2.2 Quantum correlations, Entanglement and Coherence

In this section we review the definition and properties of the quantum correlations and entanglement quantifiers studied in the paper.

Quantum correlations: Perhaps the most familiar quantum information concept which has proved a powerful tool in the study of quantum correlations in many-body system is the well known von Neumann entropy. Given a pure state, the von Neumann entropy of a reduced density matrix has information about the quantum correlations between the partition and the rest of the system. In systems of indistinguishable particles, a partition of the system could be defined in different forms: (i) a partition between two sets A and B of modes of the system, performed through partial trace over one of the sets, or (ii) a partition between the n and $N-n$ particles of the system, performed through the partial trace of $N-n$ particles on the state. The first approach provides information about the quantum correlations between the modes of the system, while the second one concerns the quantum correlations among the particles [46–62]. These two notions of quantum correlations are complementary, and the use of one or the other depends on the particular situation under scrutiny. For example, if one is interested in certain quantum information protocols a description in terms of modes might be more appropriate, while correlations in eigenstates of a many-body Hamiltonian could be more naturally described by its particle perspective. In this work we deal exclusively with the particle framework.

We define in this way the quantum correlations between the set of n and $N-n$ particles in a pure state as,

$$Q_n\left(|\psi\rangle\langle\psi|\right) = S(\hat{\rho}_n), \tag{2.7}$$

where $S(\hat{\rho}_n) = -Tr(\hat{\rho}_n \log(\hat{\rho}_n))$ is the von Neumann entropy of the n-particle reduced density matrix. It is worth making a few observations. Since the system is composed of indistinguishable fermions, due to the antisymmetrization of the wavefunction, Q_n is never null. However, for states described by a single Slater determinant (an uncorrelated fermionic state), the n-particle RDM $\hat{\rho}_n$ is a maximally mixed state over the $\binom{N}{n}$-dimensional subspace of occupied n-particle states. This results in a non-zero minimum entropy, $Q_{n,\min} = \ln \binom{N}{n}$. This minimum entropy is not zero precisely due to the antisymmetrization postulate and can be interpreted as the "exchange correlations". Any state that is not a single Slater determinant (i.e., a correlated state, typically a superposition of determinants) will have $Q_n > Q_{n,\min}$. Therefore, the difference $Q_n - Q_{n,\min}$ is the significant term that quantifies correlations beyond those strictly required by the Pauli principle.

One can show [82, 83] that the von Neumann entropy of the reduced state, and consequently our quantum correlation quantifier, is bounded as follows:

$$\ln \binom{N}{n} \leq Q_n \left(|\psi\rangle\langle\psi|\right) \leq \ln \binom{d}{n} \tag{2.8}$$

where d is the number of single-particle degrees of freedom in the system ($d = 2L$ in our system). The minimum is reached if and only if the pure state $|\psi\rangle$ can be described by a single Slater determinant.

Quantum coherence: In quantum mechanics the coherence of a state is a direct manifestation of the quantum superposition principle. Despite its fundamental importance in quantum theory, only more recently its proper quantification and characterization have been formalized [84], and a few different measures of quantum coherence were proposed. In this work we concentrate on the analysis of the ℓ_1 *norm of coherence*, defined by the integration of the absolute value of the off-diagonal matrix elements,

$$C_{\ell_1}^{[n]}(\hat{\rho}_n) = \sum_{i \neq j} |(\hat{\rho}_n)_{i,j}|. \tag{2.9}$$

We notice that this particular quantifier is basis dependent.

Entanglement spectrum: The entropy of the reduced density matrix, as discussed previously, provides useful information about the correlation among the constituents of the system. It was realized however that further insights about the many-body properties of the system can be obtained from its spectral structures. Specifically, given the reduced density matrix $\hat{\rho}_n$, it can be diagonalized as $\hat{\rho}_n = \sum_i e^{-\xi_i} |i\rangle\langle i|$, with $\xi_i \leq \xi_{i+1}$. Writing $\hat{\rho}_n = e^{-\hat{H}_n}$, we see that ξ_i and $|i\rangle\langle i|$ can be regarded as eigenvalues and eigenvectors of a fictitious n-body Hamiltonian $\hat{H}_n$. Many efforts have been devoted studying the entanglement spectrum in spatial partitions of ground state wavefunctions, leading e.g. to a better understanding of bulk-edge properties in topological insulators and superconductors [8–10].

We study in this thesis the entanglement spectrum in particle partitions, a subject much less explored so far [26–28] (see also [85] for momentum partitions or [24, 86] for

hybrid spatial/particle partition approaches), focusing on its entanglement gap,

$$\Omega_n = \xi_2 - \xi_1. \tag{2.10}$$

and analysis of the dominant eigenvector of the reduced state, i.e., the one corresponding to the largest eigenvalue.

Cumulant matrix: The cumulant matrix $\hat{\Delta}_2$, as defined in Eq.(2.6), contains the two-particle information that cannot be obtained from the single particle reduced density matrix ($\hat{\rho}_1$), or in other words, from single-particle observables. It describes in this way fundamental two-particle correlations in $\hat{\rho}_2$, also called as irreducible two-particle correlations [87]. We study the contribution of such correlations from the ℓ_1 norm of the cumulant matrix, defining the n-particle irreducible correlation as follows,

$$D_n \equiv ||(\hat{\Delta}_n)||_1 = \sum_i |\lambda_i| \tag{2.11}$$

with λ_i the eigenvalues of the cumulant matrix. It is worth noting that for states described by a single Slater determinant, cumulants of any order vanish [87], $\hat{\Delta}_n = 0$ for $2 \leq n \leq N-1$, thus leading to null particle irreducible correlations.

2.3 Subspaces sizes

The dimension of the total antisymmetric subspace of the Hilbert space for two particles corresponds to $d_2 = \binom{2L}{2}$. This space can be split into singlet and triplet subspaces.

The fraction of the dimension for the singlet subspace (s_0) is given by:

$$\frac{d_{s_0}}{d_2} = \frac{L(L+1)}{2}\binom{2L}{2}^{-1} = \frac{L+1}{4L-2} \tag{2.12}$$

which in the thermodynamic limit $L \to \infty$ reduces to $\lim_{L\to\infty} d_{s_0}/d_2 = 1/4$.

Similarly, the dimensions for the three triplet subspaces ($t_0, t_\pm$) are given by:

$$\frac{d_{t_0}}{d_2} = \frac{L(L-1)}{2}\binom{2L}{2}^{-1} = \frac{L-1}{4L-2} \tag{2.13}$$

$$\frac{d_{t_\pm}}{d_2} = \frac{L(L-1)}{2}\binom{2L}{2}^{-1} = \frac{L-1}{4L-2} \tag{2.14}$$

All subspaces converge to the same ratio of 1/4 in the thermodynamic limit.

2.4 Symmetry of the density matrix of two particles

First, let us define the one and two particles operators named S_z and $\vec{S}^2$ respectively by the equations

$$\begin{aligned}\hat{S}_z &= \frac{1}{2}\sum_i^L \left(\hat{n}_{i\alpha} - \hat{n}_{i\beta}\right) && (2.15)\\ \hat{\vec{S}}^2 &= \frac{1}{2}\hat{N} + \frac{1}{4}\sum_{ij}^L \left(\hat{n}_{i\alpha} - \hat{n}_{i\beta}\right)\left(\hat{n}_{j\alpha} - \hat{n}_{j\beta}\right) \\ &- \sum_{ij} \hat{a}^\dagger_{i\alpha}\hat{a}^\dagger_{j\beta}\hat{a}_{i\beta}\hat{a}_{j\alpha} && (2.16)\end{aligned}$$

where $\alpha = \uparrow, \beta = \downarrow$ are the fixed spin components, and $\hat{N}$ is the total number operator. Also, let us write useful (anti)commutators identities of fermion operators:

$$\begin{aligned}\left\{\hat{a}^\dagger_{i\alpha}, \hat{a}_{j\beta}\right\} &= \delta_{i,j}\delta_{\alpha,\beta}; && (2.17)\\ \left\{\hat{a}_{i\alpha}, \hat{a}_{j\beta}\right\} &= 0; && (2.18)\\ [A, B] &= \{A, B\} - 2BA; && (2.19)\\ [AB, C] &= A\{B, C\} - \{A, C\}B; && (2.20)\\ [A, B] &= -[B, A]. && (2.21)\end{aligned}$$

From these equations it follows another useful result:

$$\begin{aligned}[\hat{n}_{i\alpha}, \hat{a}_{k\sigma}] &= \hat{a}^\dagger_{i\alpha}\{\hat{a}_{i\alpha}, \hat{a}_{k\sigma}\} - \left\{\hat{a}^\dagger_{i\alpha}, \hat{a}_{k\sigma}\right\}\hat{a}_{i\alpha} \\ &= -\delta_{ik}\delta_{\alpha\sigma}\hat{a}_{i\alpha} && (2.22)\\ \left[\hat{n}_{i\alpha}, \hat{a}^\dagger_{k\sigma}\right] &= \hat{a}^\dagger_{i\alpha}\left\{\hat{a}_{i\alpha}, \hat{a}^\dagger_{k\sigma}\right\} - \left\{\hat{a}^\dagger_{i\alpha}, \hat{a}^\dagger_{k\sigma}\right\}\hat{a}_{i\alpha} \\ &= \delta_{ik}\delta_{\alpha\sigma}\hat{a}^\dagger_{i\alpha}. && (2.23)\end{aligned}$$

Using the above equations, we can then arrive at the commutator of the spin operator $\hat{S}_z$ with the creation and annihilation operators:

$$\begin{aligned}\left[\hat{S}_z, \hat{a}_{k\sigma}\right] &= \frac{1}{2}\sum_i [\hat{n}_{i\alpha}, \hat{a}_{k\sigma}] - [\hat{n}_{i\beta}, \hat{a}_{k\sigma}] \\ &= \frac{1}{2}\left(-\delta_{\alpha\sigma}\hat{a}_{k\alpha} + \delta_{\beta\sigma}\hat{a}_{k\beta}\right) && (2.24)\\ \left[\hat{S}_z, \hat{a}^\dagger_{k\sigma}\right] &= \frac{1}{2}\sum_i \left[\hat{n}_{i\alpha}, \hat{a}^\dagger_{k\sigma}\right] - \left[\hat{n}_{i\beta}, \hat{a}^\dagger_{k\sigma}\right] \\ &= \frac{1}{2}\left(\delta_{\alpha\sigma}\hat{a}^\dagger_{k\alpha} - \delta_{\beta\sigma}\hat{a}^\dagger_{k\beta}\right). && (2.25)\end{aligned}$$

Here we want to show that if the ground state of a Hamiltonian has a $U(1)$ $\hat{S}_z$ symmetry, its two particle reduced state will also have the same symmetry. So, let's call this ground state $|\psi\rangle$ and assume that the former is true (calling our operator $\hat{G}$ for now):

$$\left[|\psi\rangle\langle\psi|, \hat{G}\right] = 0. \quad (2.26)$$

If we take a partial trace of one particle in the above equation, we have

$$\begin{aligned} Tr^{(1p)}\left[\left|\psi\right\rangle\left\langle\psi\right|,\hat{G}\right] &= 0 && (2.27)\\ \sum_{k\sigma}\hat{a}_{k\sigma}\left[\left|\psi\right\rangle\left\langle\psi\right|,\hat{G}\right]\hat{a}^{\dagger}_{k\sigma} &= 0 && (2.28)\\ \sum_{k\sigma}\hat{a}_{k\sigma}\left|\psi\right\rangle\left\langle\psi\right|\hat{G}\hat{a}^{\dagger}_{k\sigma}-\hat{a}_{k\sigma}\hat{G}\left|\psi\right\rangle\left\langle\psi\right|\hat{a}^{\dagger}_{k\sigma} &= 0 && (2.29)\\ \sum_{k\sigma}\hat{a}_{k\sigma}\left|\psi\right\rangle\left\langle\psi\right|\hat{a}^{\dagger}_{k\sigma}\hat{G}+\hat{a}_{k\sigma}\left|\psi\right\rangle\left\langle\psi\right|\left[\hat{G},\hat{a}^{\dagger}_{k\sigma}\right]& \\ -\hat{G}\hat{a}_{k\sigma}\left|\psi\right\rangle\left\langle\psi\right|\hat{a}^{\dagger}_{k\sigma}-\left[\hat{a}_{k\sigma},\hat{G}\right]\left|\psi\right\rangle\left\langle\psi\right|\hat{a}^{\dagger}_{k\sigma} &= 0 && (2.30)\end{aligned}$$

that is also true and give us a neat equation for any operator $\hat{G}$:

$$\begin{aligned}\left[\rho^{(N-1)p},\hat{G}\right]+\sum_{k\sigma}\hat{a}_{k\sigma}\left|\psi\right\rangle\left\langle\psi\right|\left[\hat{G},\hat{a}^{\dagger}_{k\sigma}\right]& \\ -\left[\hat{a}_{k\sigma},\hat{G}\right]\left|\psi\right\rangle\left\langle\psi\right|\hat{a}^{\dagger}_{k\sigma} &= 0. && (2.31)\end{aligned}$$

We can use it to derive a set of equations that must hold in an iterative way. If $\hat{G}$ is a Hermitian operator, the second and third terms can be simplified as

$$\left[\rho^{(N-1)p},\hat{G}\right]+\left(\sum_{k\sigma}\left[\hat{G},\hat{a}_{k\sigma}\right]\left|\psi\right\rangle\left\langle\psi\right|\hat{a}^{\dagger}_{k\sigma}-h.c.\right)=0, \quad (2.32)$$

which means that if the first term is zero, the parenthesis is automatically zero. If it is not the case, the difference between them have to be evaluated. For the purpose of demonstrating this, we will use the $\hat{S}_z$ operator (which is clearly hermitian) for the first test case, and using the commutation relations, we have for the left side:

$$\begin{aligned}\left[\rho^{(N-1)p},\hat{S}_z\right]& \\ +\frac{1}{2}\sum_{k\sigma}\hat{a}_{k\sigma}\left|\psi\right\rangle\left\langle\psi\right|\left(\delta_{\alpha\sigma}\hat{a}^{\dagger}_{k\alpha}-\delta_{\beta\sigma}\hat{a}^{\dagger}_{k\beta}\right)& \\ +\frac{1}{2}\sum_{k\sigma}\left(-\delta_{\alpha\sigma}\hat{a}_{k\alpha}+\delta_{\beta\sigma}\hat{a}_{k\beta}\right)\left|\psi\right\rangle\left\langle\psi\right|\hat{a}^{\dagger}_{k\sigma} &= 0 && (2.33)\\ \left[\rho^{(N-1)p},\hat{S}_z\right] &= 0. && (2.34)\end{aligned}$$

This process can be iterated just changing our state $|\psi\rangle\langle\psi|$ by $\rho^{(N-1)p}$ (the rank does not make a difference) in the eq. 2.26, and we get the same conclusion for the reduced density matrix of one less fermion each time. We see that all RDM's inherit this property including ρ^{2p} and ρ^{1p} q.e.d. This equation is basically generated by the action of the particle trace operation, in a number conserving setting. For the other operator $\hat{\vec{S}}^2$ we were not able to demonstrate analytically that ρ^{2p} can be diagonalized in the same basis, but we verified it numerically and it is shown in the results section.

3 Tensor Network Theory

3.1 Matrix Product States

Tensor Networks (TN) provide an interesting tool for studying many body systems both theoretically and numerically. The fact that the dimension of the Hilbert space exponentially increases with the number of particles is a curse in lattice models which there is still no analytical solution available. Algorithms based on TN can then provide a useful framework for such complex systems e.g. topologically ordered phases, quantum spin liquids, etc. Also, TN methods are very flexible and are used in systems in different dimensions, of finite or infinite lattice sizes, translationally invariant, with open/periodic boundary conditions, states with symmetries, fermionic/bosonic systems. Another direction of recent studies using TN techniques is the relation to the holographic principle and the AdS/CFT correspondence in quantum gravity [88–94]. We cite as examples the most known Tensor Networks ansatz: *Matrix Product State* (MPS) [95–97], *Projected Entangled Pair States* (PEPS) [98] and the *Multiscale Entanglement Renormalization Ansatz* (MERA) [99, 100].

In this chapter, the main references used are [101–105]. We first cover useful notation of tensor networks showing basic properties needed in the MPS representation. In the second part of the chapter we develop an algorithm to find the ground state of any one-dimensional Hamiltonian, in which the desired accuracy is controlled by the amount of entanglement present in corresponding obtained state.

3.2 The Penrose Notation

Tensors are generalizations of matrices or vectors, i.e. a multidimensional array containing complex numbers. You can think of them as an element of $\mathbb{C}^{d_1 \times \cdots \times d_r}$, where d_i is the ith dimension of a rank r tensor, or imagine an object which you give a set of defined indices (e.g. $\{i_1 = 1, i_2 = 4, ..., i_r = 0\}$ where the indices run from 0 to $d_i - 1$) and it gives you a complex number back. This is all there is to it. But students of general relativity may remember that dealing with multiple tensors, explicitly writing all indices, can be a very harsh task to follow. The Penrose graphical notation (also called tensor diagram notation) is a visual representation of tensors that was first proposed by Roger Penrose [106], and came to simplify this task. This graphical notation is very simple, tensors are geometrical shapes (we use a square) with legs (or wires) representing their indices. Therefore, a vector can be represented by a square with one leg, a matrix is a square with two legs and so on. We only care if the vector is a *ket* or *bra*, the difference being legs facing different directions, e.g. downward and upward respectively. We put textual indications on the

tensors and their legs and then we have a didactic way to show and explain manipulations applied to these objects. See figure 2 for some examples.

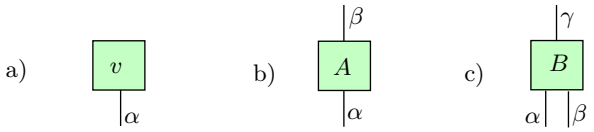

Figure 2 – TN representation of a) a vector v_α, b) a matrix A^β_α and c) a tensor $B^\gamma_{\alpha\beta}$.

Operations on tensors also have a simple representation. For example, multiplying a matrix with a vector is equivalent to sum the repeated index in

$$\sum_{\alpha}^{d_\alpha} A^\beta_\alpha v_\alpha = u_\beta, \tag{3.1}$$

which is equivalent to connect the leg of the tensors with the same index - see diagram a in fig. 3. The outer product (generalization of tensor product for vectors) is the point-wise product of values of each tensor

$$[A \otimes B]_{i_1,\ldots,i_{r_A},j_1,\ldots,j_{r_B}} = A_{i_1,\ldots,i_{r_A}} \cdot B_{j_1,\ldots,j_{r_B}}, \tag{3.2}$$

and is represented by placing the tensors next to each other, no indices are contracted - see diagram b in fig. 3. Einstein's notation is always implicit in a TN, we just replace the sum on repeated indices by connecting the legs of the tensors. When replacing them with the resultant tensor we say that the indices were *contracted* (diagram a in fig. 3 shows an index α being contracted).

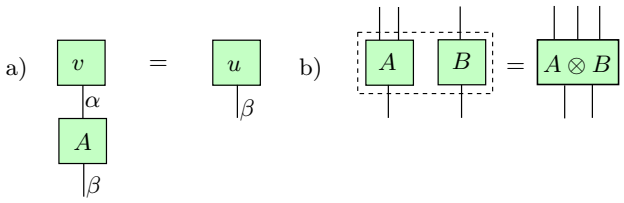

Figure 3 – a) A matrix A multiplying a vector v and b) the outer product of A and B.

The trace or the partial trace can be done just connecting the legs of the dimensions being traced out. Figure 4a shows a generic tensor that may represent a density operator of two particles in which the second has been traced out:

$$\rho_1 = Tr_2\left[\rho\right] = \sum_{i_2,i_2'} \rho\delta_{i_2,i_2'}. \tag{3.3}$$

Another operation used very often is *grouping/splitting* indices, decreasing/increasing the rank of the tensor and reorganizing its elements. This permits to reduce the rank of a tensor, allowing to generalize some linear algebraic notions defined on matrices (such

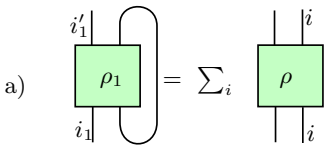

Figure 4 – Trace of a tensor.

as eigen/singular value decompositions, unitarity, etc). Figure 5 show a rank-5 tensor T being transformed in a matrix by grouping its indices (represented by a thicker leg). If two arbitrary tensors have many legs being contracted, we can group together the shared legs in just one index, then group all indices not being contracted and make a simple matrix multiplication over the resulting matrices. Subroutines perform exactly this operation when contracting multiples indices.

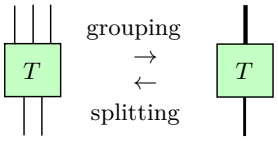

Figure 5 – Grouping and splitting operations on a generic tensor T.

The form how the grouping is done is arbitrary. It can be for example a higher-dimensional generalization of column-major ordering. The product $|0\rangle \otimes |1\rangle = |01\rangle$ is similar: a 2×2 dimensional rank-2 vector being mapped in one rank-1 4-dimensional vector using the Kronecker product as the grouping operation. The most important example of how grouping can be useful in TN is the Singular Value Decomposition (SVD). Any matrix has a unique SVD:

$$X = USV^\dagger, \tag{3.4}$$

where U and V are isometric ($U^\dagger U = VV^\dagger = \mathcal{I}$), and S is diagonal and contains the singular values. We then generalize the SVD to tensor using the grouping and splitting operations (fig. 6). The method used to group indices do not make difference, being implicit in the overall SVD operation. This central operation allows quantum state representations with low entanglement as we will see later - which uses low rank approximation of a matrix

$$X^{(k)} = US^{(k)}V^\dagger. \tag{3.5}$$

We gave the very basics of tensor network notation. A tensor network can be any combination of tensors with shared legs. When there are many tensors with legs being contracted, it is hard to determine how the most computationally fast way to do it. Time and memory performance are important facts to construct an optimized algorithm and overcome time-consuming routines. Often the cost of this procedure is represented by the number of operations performed by the computer, which depends on the underlying graph and is NP-complete. In the specific case of the variational-MPS, the best way of contraction is already known and used here.

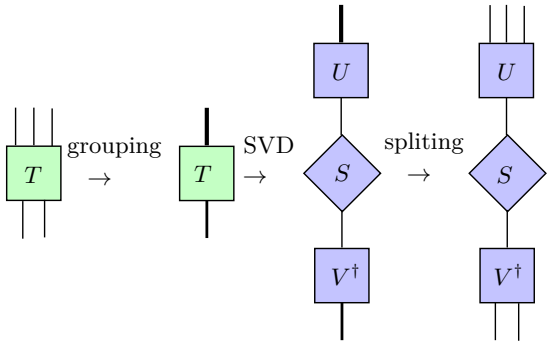

Figure 6 – General Singular Value Decomposition using the grouping and splitting operations.

3.3 Matrix Product State Representation

The pure state of a many-body system of N qudits can be described in the most general form as

$$|\psi\rangle = \sum_{i_1,\ldots,i_N}^{d} C_{i_1,\ldots,i_N} |i_1\rangle \otimes |i_2\rangle \cdots \otimes |i_N\rangle \,, \tag{3.6}$$

with $C_{i_1,\ldots,i_N} \in \mathbb{C}$ and $|i_1\rangle \otimes |i_2\rangle \cdots \otimes |i_N\rangle$ a given basis. In TN notation this state is represented by a big rank-N tensor C with d^N complex elements - where d is the dimension of each part. As mentioned before, the tensor C may be very computationally costly for our present computers if N is reasonably big. As an example, we start constructing an MPS representation of a system of 4 qudits, grouping the indices i_2, i_3 and i_4 and performing a SVD in order to get the Schmidt decomposition (fig. 7):

$$|\psi\rangle = \sum_i \lambda_i |L_i\rangle \otimes |R_i\rangle \,, \tag{3.7}$$

where $\{|L_i\rangle\}$ and $\{|R_i\rangle\}$ are orthonormal set of vectors and λ_i the Schmidt weights. The singular values of the decomposition correspond to the Schmidt weights, and we can see that this structure captures the entanglement along this cut. The values of non-zero Schmidt weights can be used to calculate the von Neumann entropy along the parts. We keep performing the SVD in each leg, and the result is shown in figure 7.

We end up with another exact representation of a state of 4 qudits that captures the entanglement structure between the chain. If we contract the singular values into the local tensors $M^{(i)}$ we get the Matrix Product State representation of the state. Then, if we have a small Schmidt rank between qudits along the chain, say D non zero Schmidt weights, we truncate the diagonal matrices $\lambda^{(i)}$ with only this D values, and truncate the matrices $M^{(i)}$ with only the important orthonormal vectors of the sets $\{|L_i\rangle\}$ and $\{|R_i\rangle\}$. Now we have only $\mathcal{O}(dND^2)$ coefficients which is polynomial in N and overcome the exponential cost of the exact representation.

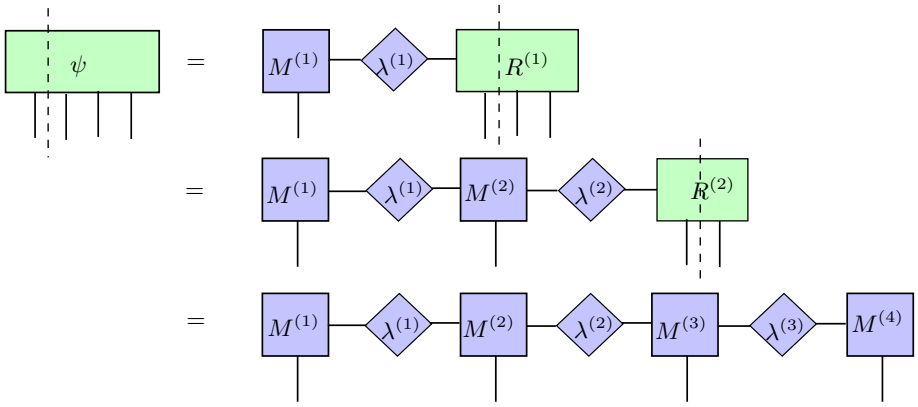

Figure 7 – Matrix Product State algorithm to represent a state of 4 particles.

Therefore, we state the affordable Matrix Product State ansatz, in periodic and open boundary conditions, given by:

$$OBC : |\psi[A]\rangle = \sum_{i_1,\ldots,i_N} A^{(1)}_{i_1} A^{(2)}_{i_2} \ldots A^{(N)}_{i_N} |i_1, i_2, \ldots, i_N\rangle , \tag{3.8}$$

$$PBC : |\psi[A]\rangle = \sum_{i_1,\ldots,i_N} Tr\left[A^{(1)}_{i_1} A^{(2)}_{i_2} \ldots A^{(N)}_{i_N}\right] |i_1, i_2, \ldots, i_N\rangle . \tag{3.9}$$

They are represented in figure 8. We see that we have the *physical indices* $i_1, i_2, \ldots, i_N$ and legs between the tensors A^i that are called *virtual* or *bond links* (they are implicit in the matrix multiplication in eqs. 3.8 and 3.9). These bond links have dimension D, which determines the maximum amount of entanglement the MPS can capture across any cut on the chain. In this dissertation, we will use the Open Boundary Conditions form of the MPS representation.

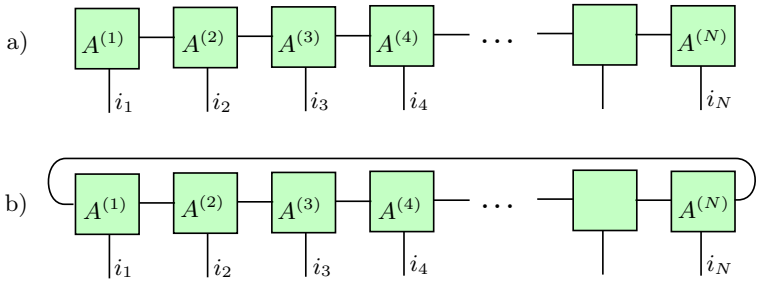

Figure 8 – Matrix Product State representation with a) Open Boundary Conditions or b) Periodic Boundary Conditions.

3.4 Gauge Freedom and Canonical Form

At this point, a quantum state $|\psi\rangle$ may be written in different MPS representations. We can insert non singular matrices $MM^{-1} = \mathcal{I}$ with dimensions $D \times D$ on the bond links, define new matrices

$$B^{(1)} = A^{(1)}M, \quad B^{(i)} = M^{-1}A^{(i)}M, \quad B^{(N)} = A^{(N)}, \tag{3.10}$$

and thus form a new MPS representation of the same state as shown in figure 9. We can even choose different $M^{(i)}$ for each bond link.

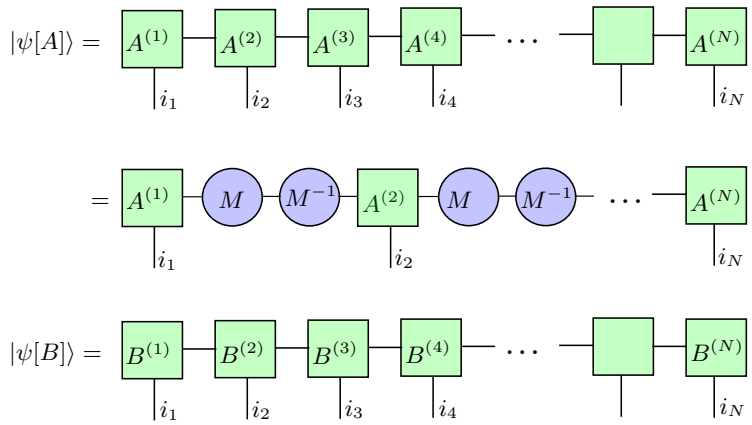

Figure 9 – MPS gauge freedom of a state.

We then define a canonical form of the MPS representation. The canonical form can be obtained by recursively applying SVD's in the MPS, starting in the first site to the penultimate site (figure 7 is a good example). Each time a SVD ($A^{(i)} = U^{(i)}S^{(i)}V^{\dagger(i)}$) is performed (always organizing the singular values in decreasing order) we define the new matrices $A'^{(i)} = U^{(i)}$ and $A'^{(i+1)} = S^{(i)}V^{\dagger(i)}A^{(i+1)}$. At the end we say that the MPS is in the *left-canonical* form which satisfies

$$\sum_j A_j^\dagger A_j = \mathcal{I}_{D\times D}. \tag{3.11}$$

Alternatively, we may start performing SVD's in the last site to the second site, defining the new matrices $A'^{(i)} = V^{\dagger(i)}$ and $A'^{(i-1)} = A^{(i-1)}U^{(i)}S^{(i)}$. Thus we say that the MPS is in the *right-canonical* form which satisfies

$$\sum_i A_j A_j^\dagger = \mathcal{I}_{D\times D}. \tag{3.12}$$

In both canonical forms the matrices obey the constraints shown in figure 10. As we will see, the variational algorithm starts with a MPS filled with random entries. The first step is to perform this algorithm to put the MPS in one of the canonical forms. The matrix that remained unused ($A^{(1)}$ for the right-canonical form and $A^{(N)}$ for the left-canonical form) is the start point of the variational algorithm, therefore it does not matter which constraint it initially obeys. Also, we can use a mixed left/right isometric form putting the left (right) matrices in the left(right)-canonical form taking as reference a particular site in the middle of the chain.

3.5 Mixed States and Matrix Product Operators

Given a MPS representation of a pure state $|\psi\rangle$, we can represent its density matrix $\rho = |\psi\rangle\langle\psi|$ just by placing the ket and bra vectors next to each other (fig. 11). It is useful

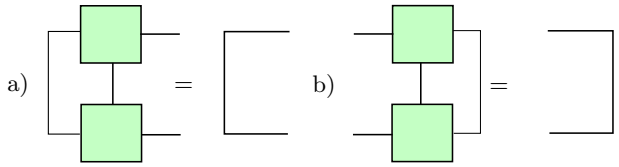

Figure 10 – MPS (a) left-canonical form and (b) right-canonical form constraints.

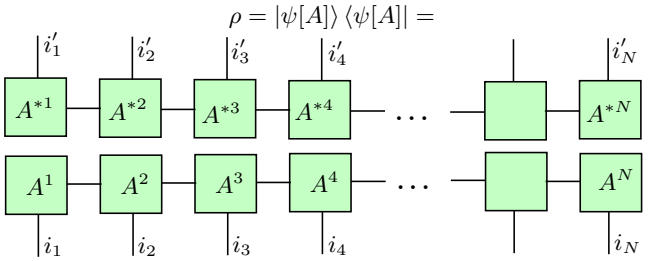

Figure 11 – Graphical representation of the density matrix $\rho = |\psi\rangle \langle\psi|$.

to obtain the reduced density matrix of a few sites of the chain. As an example, suppose we want the density matrix of particles at the positions $i = 2$ and $i = 4$. We use the trace operation and contract all the other indices as shown in figure 12a. If the MPS representation is in the right gauge for $i > 4$ and in the left gauge for $i < 2$, the cost of this operation is extremely reduced as many contractions give identities (fig. 12b). This

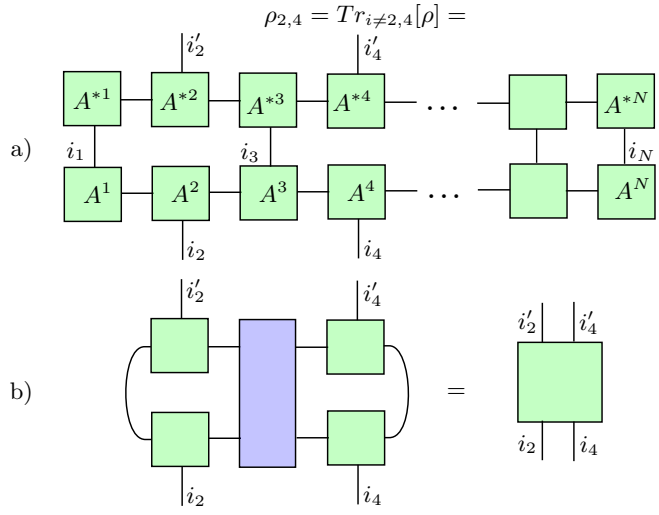

Figure 12 – MPO density matrix representation of two particles.

reduced density matrix representation is an example of a *matrix product operator* (MPO), defined in a general form in figure 13. The Quantum Ising Hamiltonian

$$H = -J \sum_{i}^{N-1} \sigma_i^x \sigma_{i+1}^x - g \sum_{i}^{N} \sigma_i^z \tag{3.13}$$

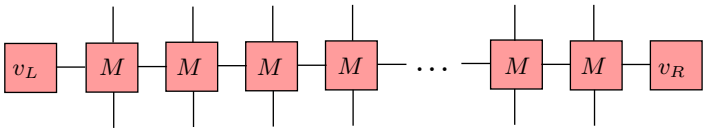

Figure 13 – MPO graphical representation.

is represented with the MPO's

$$M = \begin{pmatrix} \mathcal{I} & 0 & 0 \\ \sigma^x & 0 & 0 \\ -g\sigma^z & -J\sigma^x & \mathcal{I} \end{pmatrix}, \quad v_L = (0\ 0\ 1), \quad v_R = \begin{pmatrix} 1 \\ 0 \\ 0 \end{pmatrix}. \tag{3.14}$$

The Hamiltonian in this representation is simply given by $H = v_L M^N v_R$.

3.6 Variational-MPS Algorithm

Our aim is to find the ground state of a one-dimensional Hamiltonian in the MPS representation. The Quantum Ising MPO of the previous section is an example of such Hamiltonian, and are represented by red squares in TN notation of all figures in this section. We use a variational approach that minimizes the Rayleigh quotient

$$|GS\rangle \equiv \min_{|\psi\rangle \in \mathcal{D}} \frac{\langle\psi| H |\psi\rangle}{\langle\psi|\psi\rangle}, \tag{3.15}$$

where the domain $\mathcal{D}$ is composed by states that are well-approximated by MPS. The steps to reach the ground state are summerized as: (1) first we guess a MPS, (2) then we minimize the Rayleigh quotient choosing just one site of the MPS as a variable, (3) we proceed to the next sites performing the previous step until we went through all the chain and finally (4) test if the energy converged.

In the first step, we can set each $A^{(i)}$ matrix with random numbers, and set the MPS in the right-canonical form. In steps (2) and (3) we start in the first site passing through the chain to the end, and then went back passing through the chain to the first site (we say that a *sweep* was performed). A generic step is represented in figure 14, where the tensor $A^{(i)}$ is the variable and all other tensors are fixed. In this process of contracting

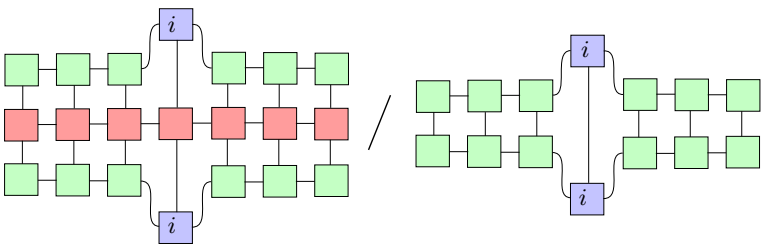

Figure 14 – Rayleigh quotient in TN notation.

all the fixed tensors into just one, we define *environment tensors* shown in figure 15. We rewrite the minimization process as

$$A^{(i)} \leftarrow \min_{A^{(i)}} \frac{\left\langle A^{(i)} \right| H_{eff}^{(i)} \left| A^{(i)} \right\rangle}{\left\langle A^{(i)} \right| I^{(i)} \left| A^{(i)} \right\rangle}. \tag{3.16}$$

If the sites in the left of site i are in the left-canonical form, and those to the right are in

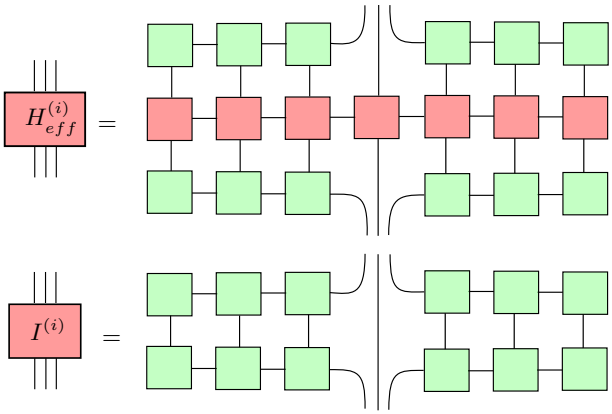

Figure 15 – Environment tensors definition.

right-canonical form, the environment tensor $I^{(i)}$ reduces to the identity as shown in figure 16. Therefore, as we move along the chain we change the canonical form of the matrices in order to satisfy this requirements. The minimization process simplifies to

$$A^{(i)} \leftarrow \min_{A^{(i)}} \frac{\left\langle A^{(i)} \right| H_{eff}^{(i)} \left| A^{(i)} \right\rangle}{\left\langle A^{(i)} | A^{(i)} \right\rangle}. \tag{3.17}$$

$H_{eff}^{(i)}$ is hermitian and the minimization solution is given by its eigenvector with minimum

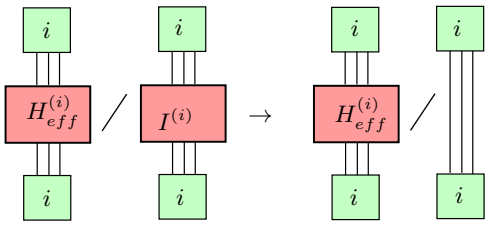

Figure 16 – Simplification in the minimization process.

eigenvalue. The eigenvalue/eigenvector is calculated using the grouping operation in $H_{eff}^{(i)}$ transforming it into a matrix, and then using Matlab subroutines such as eigs/schur which quickly solve for the minimum eigenvalue. Finally, in step (4) we compare the energy between the sweeps and stop after the difference reaches some threshold. It may seem that H_{eff} is very expensive to compute in each minimization step, as there are many legs to contract in the whole tensor. First, we mention before that is already known the quickest way to perform the contraction. Also, we can divide H_{eff} in three tensors as

shown in figure 17, where $L^{(i)}$ refers to the contraction of every tensor to the left of site i, $R^{(i)}$ refers to the contraction of every tensor to the right of site i, and $M^{(i)}$ the MPO of the corresponding site. Before the minimization process begin in the first site, $R^{(i)}$ is calculated for every site. As we move through the chain $L^{(i)}$ is recursively calculated using the resultant matrices $A^{(i)}$ of the minimization process. This recursive update is the reason the computational cost is considerably reduced: $H^{(i)}_{eff}$ is easily obtained from the stored $L^{(i)}$, $R^{(i)}$, and $M^{(i)}$ tensors without re-contracting the entire chain for each site.

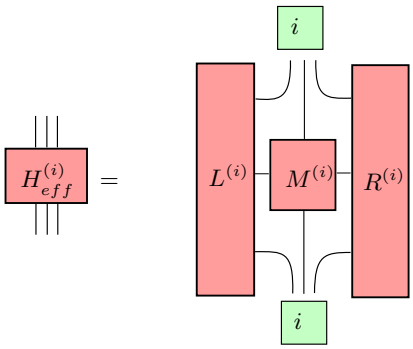

Figure 17 – Decomposition of $H^{(i)}_{eff}$.

3.7 Simulation Parameters

In order to obtain numerically the ground states of the EHM and its particle reduced density matrices, we use the Matrix Product State (MPS) ansatz, which can be a faithful representation of systems in one dimension with local interactions. The method can be accomplished by mapping the fermionic model to a spin-half system, i.e., representing the fermionic operators with a Jordan-Wigner transformation [107], that preserves the anti-commutation relations, and thus recovering the usual tensor product Hilbert space structure needed for the implementation of MPS. The variational algorithm to minimize energy was performed using the Density Matrix Renormalization Group (DMRG), which is standard in such a task. In our calculations we used 20 sweeps in the minimization process, which proved enough for the energy convergence of the order of at least $\mathcal{O}(10^{-8})$ and up to $\mathcal{O}(10^{-16})$, depending on the region of the phase diagram and the system size. We also implemented a fast and efficient algorithm to calculate correlators of fourth order, needed to construct the 2-particle RDM's. The MPS representation accuracy was controlled by two parameters, χ and D, corresponding to the *minimum allowed singular value permitted* and the *bond link* (size of the virtual dimension of the matrices), respectively. Whereas we use an adaptive algorithm which increases the bond link as needed, $\chi \approx \mathcal{O}(10^{-20})$ is the minimum singular value considered and $D = 2000$. All quantities computed in this article have not significantly changed for larger bond links ($D \sim 4000$), indicating a very good precision to the calculations. *E.g,* the entanglement gap, which is the subtler quantity

under study, has changed its value only at the order of $\mathcal{O}(10^{-12})$ thus validating a good precision. We consider open boundary conditions in the model because it is best suited to the MPS formalism and finite-size scaling analysis.

4 Results

4.1 Resume

With all the tools we have crafted, we now face the challenge to study the quantum phase transitions present in the Extended Hubbard Model and show our results for the model. In a short resume, our quantifiers capture most of the quantum phase transitions of the model, with exception to some BOW related phase transitions. The quantifiers show peculiar behaviors such as discontinuities, maximum or minimum values at the quantum phase transitions.

It is interesting to interpret such behaviors based on the order parameters for the different phases of the model. As discussed in Sec.(1.2), the different phases are characterized by their order parameters $\hat{O}_i$ (e.g. charge-operator (CDW), spin-operator (SDW) and others) and corresponding correlators $\langle \hat{O}_i \hat{O}_j \rangle$. These correlators correspond to specific elements of the RDM. On the verge of a second-order phase transition the correlator's correlation length, which is an implicit function of the Hamiltonian gap, tends to diverge. Therefore, these terms will be dominant in the RDM and a peculiar behavior of our quantifiers is also expected along these transitions, corroborating with our numerical results. Although there is an implicit connection between the order parameter correlators, the Hamiltonian gap and our quantifiers, the latter will in general correspond to intricate functions of the RDM elements, thus not necessarily implying a clear (linear) connection among all these properties. In fact we find (as we discuss in more detail below) that some quantifiers may be more sensitive to certain transitions than others, thus working in a complementary form in order to describe the phase diagram of the model.

4.2 Quantum Phase Transitions

In Fig.(18) we show the quantum correlations (Q_2) and irreducible correlations (D_2) for the phase diagram of the model. We see that both the quantum correlations of 2 fermions with the rest of the $N-2$ particles (Q_2) as well the correlation between the reduced 2 fermions (D_2) in the reduced state behave qualitatively similar, showing discontinuities at the 1st order transitions of the model, while are continuous reaching minimum values at the 2nd order phase transitions.

In Fig. (19) we show the quantum coherence (C_2) in the reduced density matrices. We recall that the coherence here is computed in the real space basis. While at 1st order transitions C_2 also display discontinuities, at the 2nd order phase transitions it presents

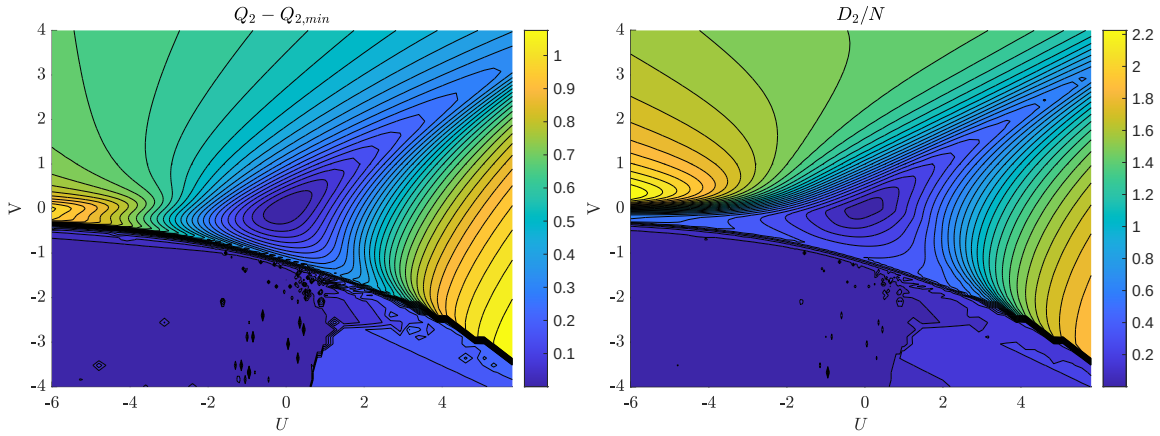

Figure 18 – Results for the two-body reduced density matrix in a system at half filling ($N = L$ fermions) along the full phase diagram of the model. We show the quantum correlations Q_2 and the irreducible two-body correlations D_2. We consider a system with $L = 16$ sites. We see that these quantities capture most of the quantum phase transitions of the model, *e.g* displaying discontinuities at 1st order transitions and continuous maximum/minimum values at 2nd order transitions.

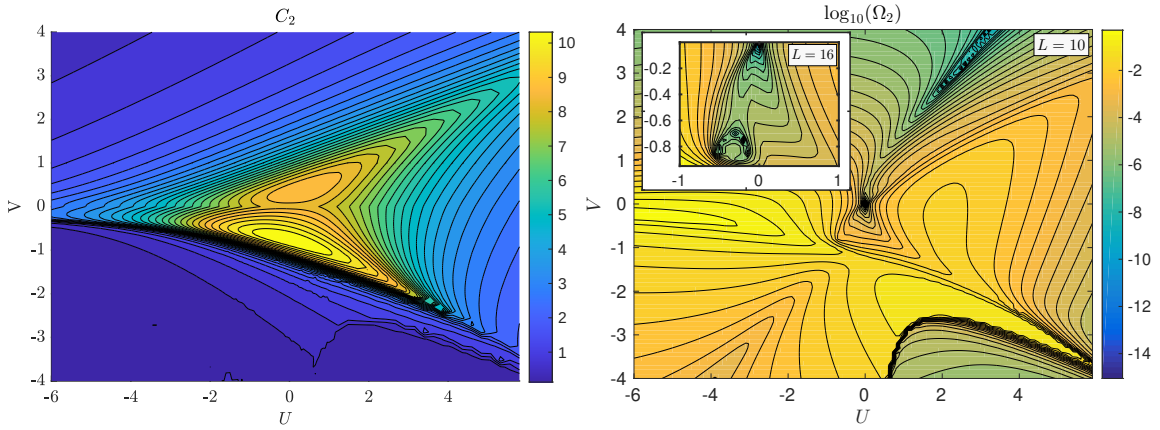

Figure 19 – Results for the two-body reduced density matrix in a system at half filling ($N = L$ fermions) along the full phase diagram of the model. We show the coherence C_2 and the entanglement gap Ω_2. We consider a system with $L = 16$ sites with exception to the entanglement gap main panel, which we use a system with $L = 10$ sites for the complete phase diagram, and highlight in the inset its behavior for larger $L = 16$ sites across the superconducting region. We see that all these quantities capture most of the quantum phase transitions of the model, *e.g* displaying discontinuities at 1st order transitions and continuous maximum/minimum values at 2nd order transitions.

maximum values. Since coherence is a basis dependent quantity, and we work at the real space representation for the reduced density matrix, at the quantum phase transitions we expect it to be maximum due to the divergence of the coherence length.

We also show in Fig. (19) the entanglement gap (Ω_2). Even though the eigenvalues of the reduced density matrix can be gapless, the two "dominant" excitations contain relevant information of the phase, in the same spirit as Penrose-Onsager criterion [108, 109]. We see that the entanglement gap displays a similar behavior of maximum/minimum and discontinuities along the transitions of the model. We further notice a peculiar behavior of the entanglement gap within the superconducting phase (see inset of the right panel of Fig. (19)), suggesting a phase transition, or a change of dominant eigenvalue with the gap closing/crossing. We devote a more detailed analysis of this point in Sec. 4.2.2, highlighting the presence of a TS/SS superconducting transition. Moreover, the entanglement gap also displays an anomalous behavior in the strong coupling regions $U/V \sim 1$ with $t \ll 1$, which is not seen in the other quantifiers nor expected from the known phase diagram of the model (Fig.(1)). While for $U, V > 0$ we see a very abrupt closure of the entanglement gap, in the opposite case with $U, V < 0$ there is a less apparent (but still emergent) minimum in the quantifier. We attribute these behaviors to the different "defects" (at a few-body level) that can occur in the corresponding phases, as we discuss in Sec.(4.2.3). Depending on the ratio V/U different types of local defects prevail in the ground state wavefunction. The entanglement gap, interestingly, is more sensitive to such few-body fluctuations in the wavefunction as compared to the other quantifiers. This increased sensitivity may be a consequence of its definition, based on a restricted (the dominant) set of eigenvalues/eigenvectors of the RDM. In this way it can work as a magnifying glass on specific changes over the RDM such as those caused by few-body fluctuations, differently from the other quantifiers which are complex functions integrated over all degrees of freedom of the reduced density matrix. Since fluctuations at a few-body level are suppressed over the full degrees of freedom, they become less apparent for such quantifiers.

We discuss now in more detail the behavior of the quantifiers along specific regions of interest in the phase diagram.

4.2.1 $U/t = 4$

Along the line with fixed $U/t = 4$ and varying inter-site interactions V/t, the model shows different phase transitions, namely, PS-SDW, SDW-BOW and BOW-CDW transitions. We show in Fig.(20) our quantifiers along this line, for different system sizes. We see the behaviors for the quantifiers discussed previously. A few aspects are worth remarking. The quantifiers show two discontinuities along the PS phase. This is due to the existence of different PS phases in this region, where the fermions tend to cluster in two different structures, as discussed also in Refs. [37, 70].

We perform a finite-size scaling analysis for the interaction $V^*(L)_{[...]}$ where the quantifiers are maximum/minimum along the line, in the region $U/t > 0$, and compare with expected results for the critical interaction of the literature. We show our results in Fig.(20)-(bottom panel). We obtain that,

$$\begin{aligned} V^*(L\to\infty)_{[Q_2]} &\cong 2.22, \qquad V^*(L\to\infty)_{[C_2]} \cong 2.23, \\ V^*(L\to\infty)_{[D_2]} &\cong 2.02, \qquad V^*(L\to\infty)_{[\Omega_2]} \cong 2.24, \end{aligned} \tag{4.1}$$

It is interesting to put these results in perspective with those obtained in the literature. According to the literature, the best estimates for the quantum phase transitions in this region correspond to $V/t \approx 2.16$ [72, 73, 75–77] for the CDW-BOW transition, and $V/t \approx 1.88 - 2.00$ [72, 73, 76, 77] or $V/t \approx 2.08$ [74] for the BOW-SDW transition. We see in this that while Q_2, C_2 and Ω_2 are close to the expected CDW-BOW transition point, D_2 is closer to the BOW-SDW transition.

4.2.2 Superconducting phase

We focus here in the analysis of the superconducting phase of the model. It is convenient to first discuss a few symmetries of the model and the two-body reduced density matrix. We first define the total spin operator $\vec{S}^2$ and total spin along z-axis $\vec{S}_z$, respectively, as

$$\begin{aligned} \vec{S}^2 &= \frac{1}{2}\hat{N} + \frac{1}{4}\sum_{ij}^{L}\left(\hat{n}_{i\uparrow} - \hat{n}_{i\downarrow}\right)\left(\hat{n}_{j\uparrow} - \hat{n}_{j\downarrow}\right) + \\ &- \sum_{ij}\hat{a}^\dagger_{i\uparrow}\hat{a}^\dagger_{j\downarrow}\hat{a}_{i\downarrow}\hat{a}_{j\uparrow}, \end{aligned} \tag{4.2}$$

$$\hat{S}_z = \frac{1}{2}\sum_i(\hat{n}_{i\uparrow} - \hat{n}_{i\downarrow}) \tag{4.3}$$

with $\hat{N}$ being the total number operator. It is not hard to see that the Hamiltonian commutes with the above operators, thus possessing a $su(2)$ symmetry [110]. It is not direct that the two-body reduced density matrix should inherit the symmetries of the Hamiltonian. We notice, however, from its own definition that terms that do not conserve the total spin along z direction are null. Thus the reduced density matrix inherits at least the symmetry $\hat{S}_z$.

Interestingly, we observed numerically that the two-body reduced density also has symmetry $\vec{S}^2$, therefore indeed sharing the $su(2)$ Hamiltonian symmetry. We were not able, however, to demonstrate it analytically, rather we observed numerically along all phase diagram and for different system sizes that this property is present. The $su(2)$ symmetry in the reduced state leads to interesting consequences and avenues of investigation for

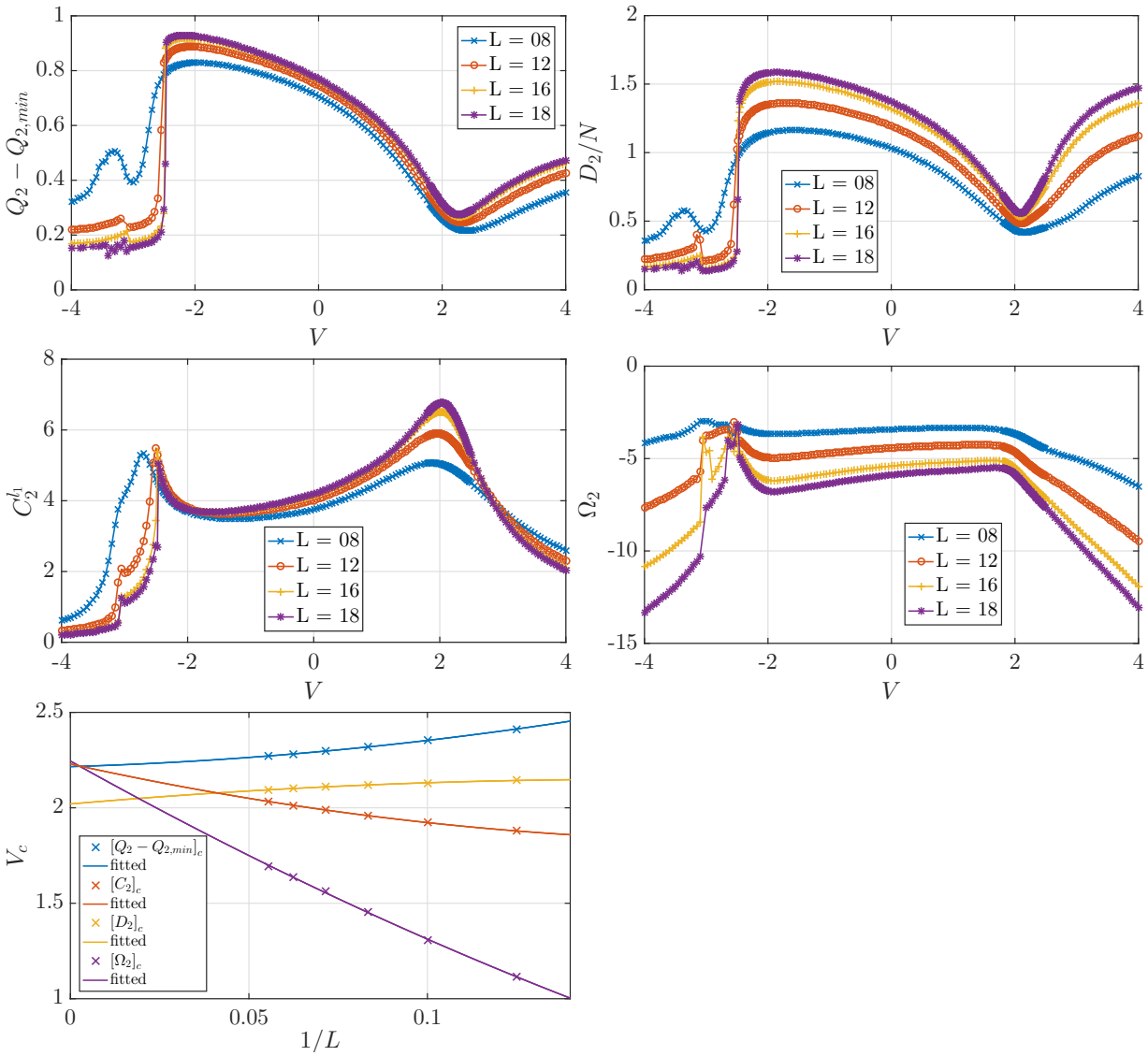

Figure 20 – Results for the two-body reduced density quantifiers along the line in the phase diagram with $U/t = 4$ fixed, for varying V/t and system sizes L, highlighting transitions between PS1-PS2-SDW-CDW. We show in **(top-left panel)** the quantum correlations Q_2, **(top-right panel)** irreducible correlations D_2, **(middle-left panel)** coherence C_2 and **(middle-right panel)** entanglement gap Ω_2. In the **(bottom panel)** we show the finite-size scaling analysis for the interactions $V(L)^*_{[...]}$ where the quantifiers are maximums, or minimums, in the region with $U/t > 0$. The fitted lines use a second order polynomial in $1/L$.

the analysis of the state in the superconducting phase. We first recall that the total spin operator commutes with $\hat{S}_z$ and split the Hilbert space of the reduced density matrix into triplet and singlet subspaces with quantum number (S^2, S_z) given by,

$$t_\pm \equiv (2, \pm 1), \quad t_0 \equiv (2, 0), \quad s_0 \equiv (0, 0) \tag{4.4}$$

where $t(s)$ denotes triplet (singlet) subspace. The dimension of the antisymmetric subspace of the Hilbert space for two particles corresponds to $d_2 = \binom{2L}{2}$. The fraction of the dimension for the singlet on such space is given by,

$$\frac{d_{s_0}}{d_2} = \frac{L(L+1)}{2}\binom{2L}{2}^{-1} = \frac{L+1}{4L-2} \tag{4.5}$$

which in the thermodynamic limit $L \to \infty$ reduces to $\lim_{L\to\infty} d_{s_0}/d_2 = 1/4$. Similarly, for triplet subspaces $t_0, t_\pm$ we have,

$$\frac{d_{t_0,t_\pm}}{d_2} = \frac{L-1}{4L-2} \overset{L\to\infty}{\longrightarrow} 1/4 \tag{4.6}$$

All subspaces converge to the same ratio of $1/4$ in the thermodynamic limit. The symmetries imply in a block diagonal structure for the reduced state in the above subspaces, and can be written as,

$$\hat{\rho}_2 = \sum_{i=s_0,t_0,t_\pm} p_i(\mathcal{P}_i \hat{\rho}_2 \mathcal{P}_i^\dagger) \tag{4.7}$$

with $\mathcal{P}_i$ the projectors onto the singlet and triplets subspaces, and $p_i = Tr(\hat{\rho}_2 \mathcal{P}_i)$ the overlap of the reduced density matrix in its respective subspace. We obtain numerically that the overlap p_i of the reduced density matrix on each subspace is constant along all phase diagram of the model, depending only on the number of sites in the system. Moreover, in the thermodynamic limit the overlap of all subspaces tend to the fraction of their dimensions over the antisymmetric Hilbert space, precisely, $p_i \to d_i/d_2 = 1/4$ for $N \to \infty$ with $i = s_0, t_0, t_\pm$ - see Fig.21.

Spectral properties. We study the spectral properties of the reduced density matrix, taking in consideration the splitting of singlet and triplet quantum numbers. We show in Fig.(22) the largest eigenvalues of the reduced density matrix in the superconducting region, for varying system sizes and on-site interactions. We see that around $U/t \sim -3$, with $V/t = -0.5$, there is a single dominant eigenvalue, corresponding to the singlet subspace. Indeed in this region we expect, according to the literature, the existence of a SS phase. As the on-site interaction is decreased (in modulus), triplet eigenvalues become comparable to the dominant singlet, until at a certain interacting value ($U^*_{ss-ts}(L, V/t)$) the triplet dominant eigenvalue surpass the singlet and becomes the largest eigenvalue. In this region we expect the dominance of a TS phase. The existence of different superconducting orderings was also studied in Refs. [70, 71, 78, 79].

In Fig.(23) we show the gap Ω_2 in the superconducting region, making clearer the regions with dominance of a SS or TS eigenvalues, as well as their dependence with system

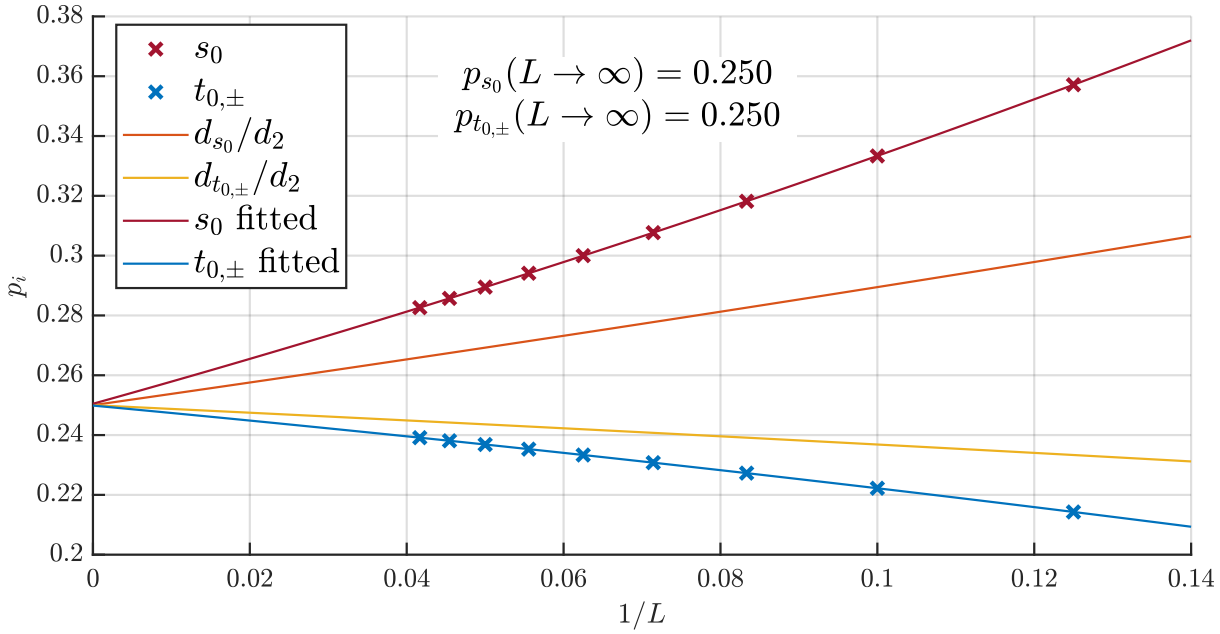

Figure 21 – Asymptotic limit of the subspaces probabilities as a function of $1/L$. The fitted lines use a second order polynomial in $1/L$.

size and interactions. We see that the critical interaction $U^*_{ss-ts}(L, V/t)$ for a change of singlet/triplet dominance increases (in modulus) for larger system sizes as well as for larger (in modulus) inter-site interaction. A quantitative analysis of the transition line between the two different superconducting phases in the thermodynamic limit ($U^*_{ss-ts}(L, V/t)$ for $L \to \infty$) is beyond the scope of this thesis. It requires the analysis of much larger system sizes, which at the moment are numerically too expensive. It is worth remarking that even though a TS phase "enlarges" in the phase diagram for increasing system sizes, the trends in our finite-size data suggest that the two different SS/TS orderings remain present in the thermodynamic limit. This analysis is based on the behavior of the entanglement gap Ω_2 (shown in Fig. 23) away from the critical point: in the region of singlet dominance (e.g., $V/t = -0.5$ and $U/t \sim -1$), the gap Ω_2 becomes larger as we increase the system size. This opening of the gap with L indicates the stability of the singlet-dominant phase. A similar trend occurs in the region of triplet dominance (e.g., for $V/t = -0.5$ and $U/t \sim -0.25$, where for large enough system sizes we see a dominance of triplet eigenvalues ($L \sim 18$ sites), and further increasing the system size the gap increases as well, corroborating the triplet eigenvalue dominance in the thermodynamic limit.

Dominant eigenvectors. We perform a deeper analysis of the dominant eigenvalue of the reduced density matrix, studying their eigenvector structure. In order to understand how the fermions are ordered within the eigenvector, we study its coherent superpositions. Specifically, we introduce a "canonical" basis in real space for the antisymmetric Hilbert

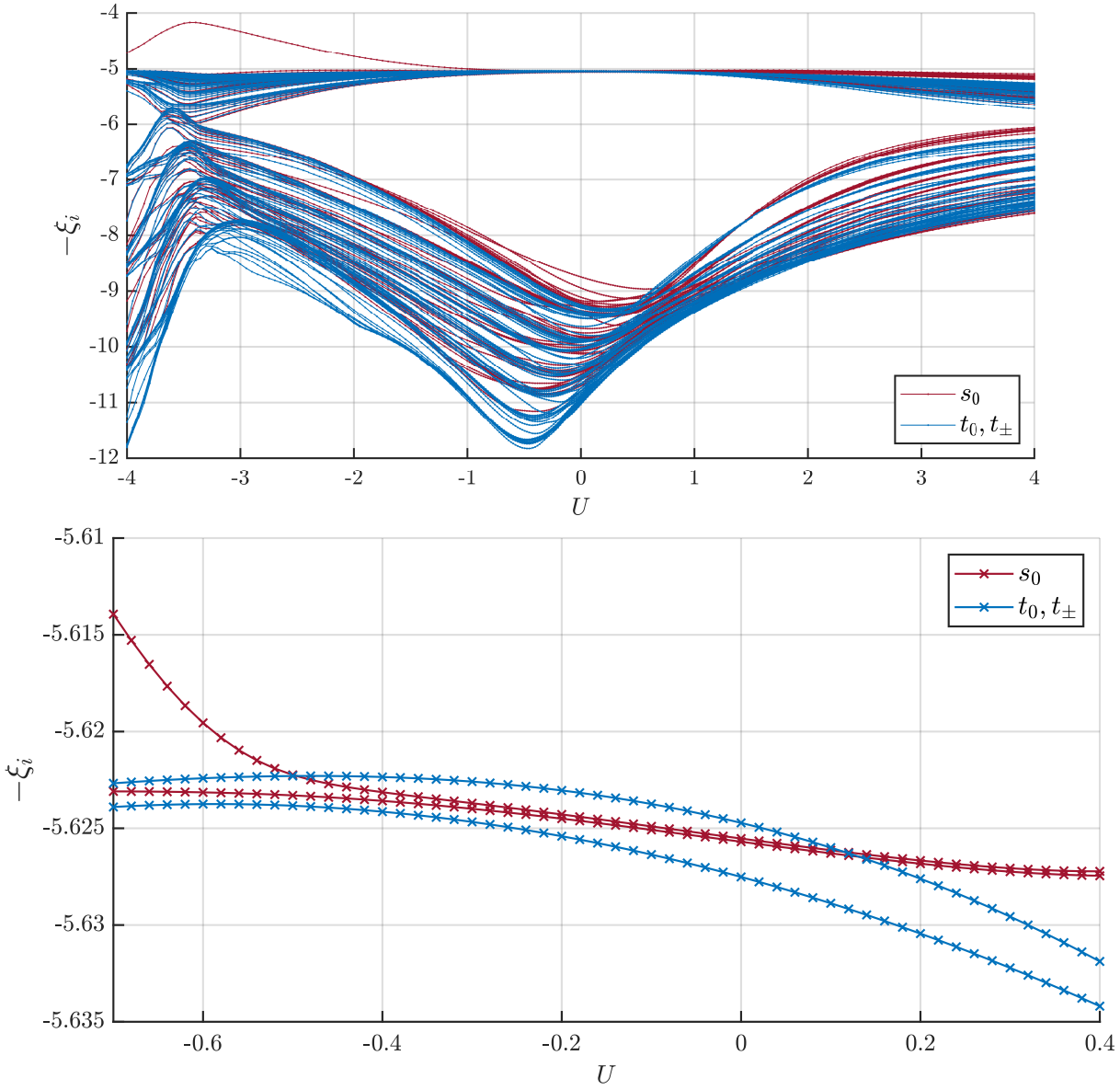

Figure 22 – Entanglement spectrum of the reduced density matrix $\hat{\rho}_2$ for a system with $L = 18$ ($L = 24$) sites and interactions $V/t = -0.5$ ($V/t = -0.6$) for the top (bottom) panel. We show here only the first 100 (8) largest eigenvalues of the spectrum. In the bottom panel, the 8 largest eigenvalues are pairwise degenerate, resulting in 4 distinct lines.

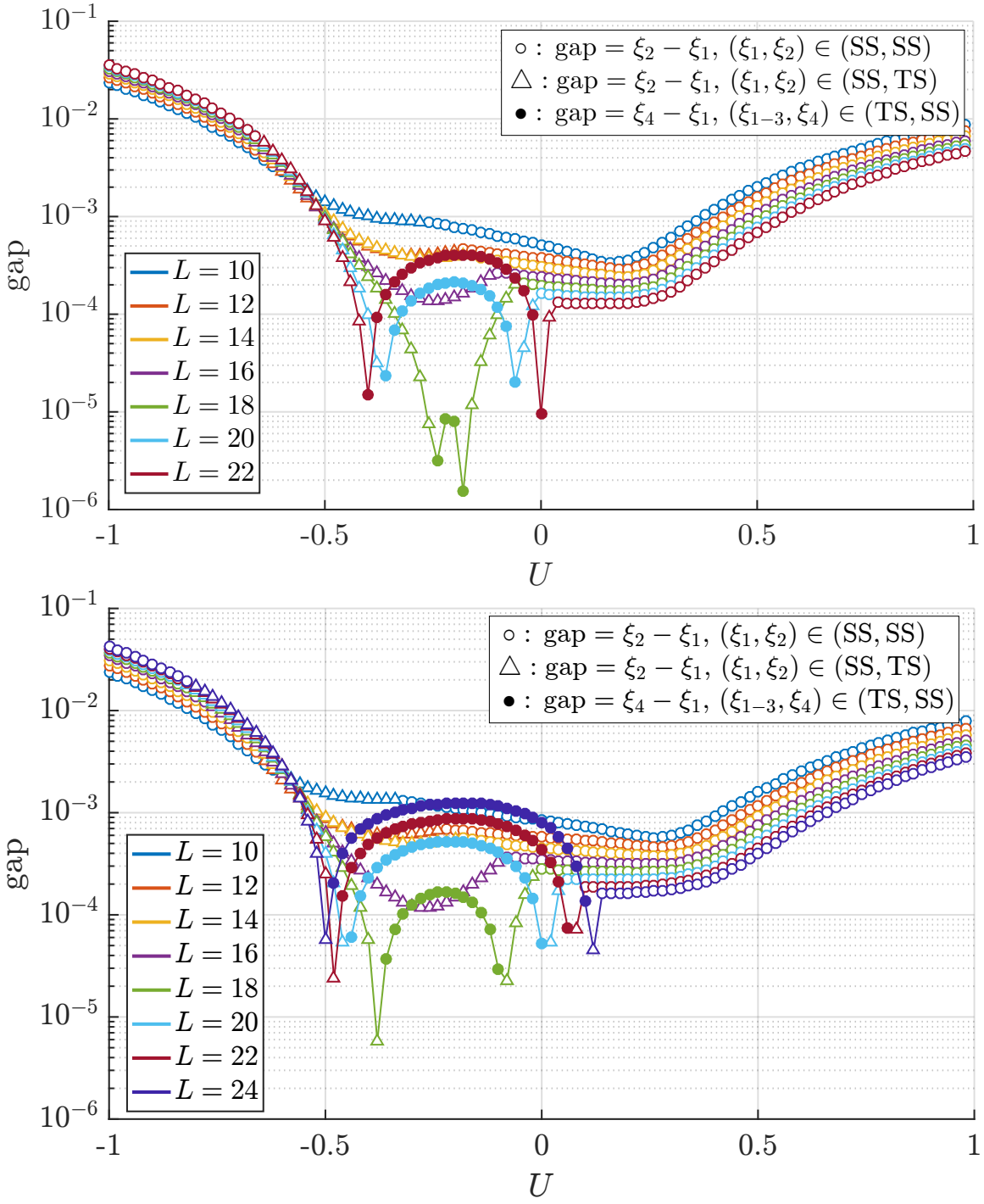

Figure 23 – Entanglement spectrum gap for the lines $V/t = -0.5$ (top) and $V/t = -0.6$ (bottom), for varying system sizes and on-site interactions. Empty (filled) symbols denote a dominant singlet (triplet) eigenvalue. In the case where the triplet is the dominant eigenvalue we have a three-fold degeneracy in the largest eigenvalues ($\xi_1 = \xi_{2,3}$) all belonging to triplet subspaces. We show in this case the gap with the next largest eigenvalue (ξ_4), according to the figure legend.

space of two-fermions, in the singlet ($|s^0_{ij}\rangle$) and triplet ($|t^{[...]}_{ij}\rangle$) subspaces, as follows,

$$|s_{0,ij}\rangle = \frac{(\hat{a}^\dagger_{i\uparrow}\hat{a}^\dagger_{j\downarrow} - \hat{a}^\dagger_{i\downarrow}\hat{a}^\dagger_{j\uparrow})}{\sqrt{2}}|vac\rangle\,, \tag{4.8}$$

$$|t_{0,ij}\rangle = \frac{(\hat{a}^\dagger_{i\uparrow}\hat{a}^\dagger_{j\downarrow} + \hat{a}^\dagger_{i\downarrow}\hat{a}^\dagger_{j\uparrow})}{\sqrt{2}}|vac\rangle\,, \tag{4.9}$$

$$|t_{+(-),ij}\rangle = \hat{a}^\dagger_{i\uparrow(\downarrow)}\hat{a}^\dagger_{j\uparrow(\downarrow)}|vac\rangle\,. \tag{4.10}$$

The dominant eigenvector $|D\rangle$ can always be decomposed in such a basis, $|D\rangle = \sum_{i,j} c_{ij} \times |s^0(t^{[0,\pm]})_{ij}\rangle$, depending if it belongs to the singlet or triplet subspace. We show in Fig.(24) the coherence profiles for the dominant eigenvector along the superconducting region. In Fig.(24)-(top left) we show the case where the system belongs to a SS phase, with interaction values $U/t = -3.4$, $V/t = -0.5$ and the dominant eigenvector belonging to the singlet subspace. In this case the coherence profile $|c_{ij}|^2$ shows an almost uniform distribution along the chain for a fixed distance $|i-j|$ between the sites, displaying in this way a coherent superposition of fermionic pairs along all the chain of the system. Moreover, the coherence is maximum for fermion pairs at the same site ($i = j$), i.e., the fermions prefer a spatially local pairing ordering. In Fig.(24)-(top right) we show now the case where the system belongs to a TS phase, with interacting values $U/t = -0.2$, $V/t = -0.6$ and the dominant eigenvector belonging to the triplet subspace. We see a similar profile with, however, a predominance of triplet pairs between nearest-neighbor sites (we recall that triplet pairs are forbidden to occupy the same site, $i \neq j$).

In Fig.(24)-(bottom pannels) we show the coherence of the dominant eigenvectors in the singlet and triplet subspaces, highlighting their dependence with the distance between the pairs. Interestingly, we notice that as we move from the SS phase towards the TS phase, the singlet pairs tend to spatially move apart from each other, while the triplet pairs tend to get closer together. This indicates that the dominance of each pairing phase is related to the distance between the fermion pairs in the model - spatially closer (and coherent) pairings prompt a stronger superconducting ordering.

4.2.3 $U \sim V$: Strong Coupling Regime ($U, V \gg t$)

Along the line with roughly equal couplings $U \sim V$ and in the strong coupling regime $U, V \gg t$ the entanglement gap displays a minimum, indicating in this way a possible phase transition in the model not yet discussed in the literature. Since they persist along the strong coupling regime, one can better analyse the system within perturbation theory picture. Along this approach we observe that there are no macroscopic changes in the properties of the ground state, rather they follow at a few-body level (different types of local defects in the wavefunction). Let us analyse the two cases, repulsive $U, V > 0$ and attractive $U, V < 0$, separately.

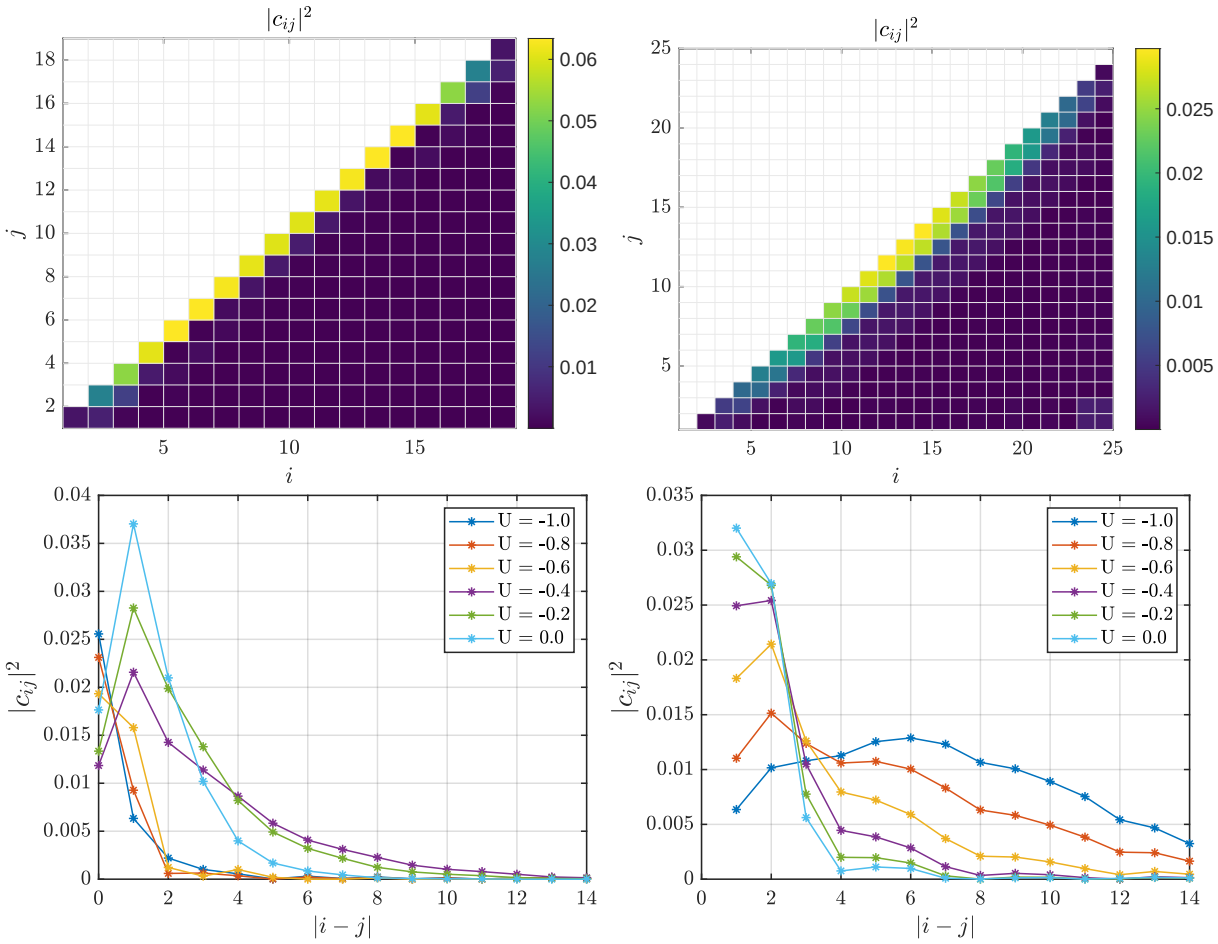

Figure 24 – Coherence profiles $|c_{ij}|^2$ for the eigenvectors of the reduced density matrix. In the top panels we show the coherence profile for the dominant eigenvector in a system with **(top-left)** $L = 18$ sites, $V/t = -0.5$, $U/t = -3.4$ and **(top-right)** $L = 24$ sites, $V/t = -0.6$, $U/t = -0.2$, in the singlet and triplet subspaces respectively. In the bottom panels we show the coherences for the dominant eigenvectors of the **(bottom-left)** singlet and **(bottom-right)** triplet subspaces, in a system with $L = 24$, $V/t = -0.6$ for varying on-site interactions. In the bottom panels, the coefficients c_{ij} are chosen close to the middle of the chain to minimize finite size effects and represent the bulk of the system (in the thermodynamic limit they will only depend on the distance $|i - j|$).

Case $U, V > 0$ (repulsive): In the region with $V \gtrsim U/2$ and considering the infinite coupling limit $t \to 0$, the ground state is characterized by macroscopic charge-density-wave configurations, such as $|2020...20\rangle$ or $|0202...02\rangle$. However, due to the open boundary conditions in the chain, these CDW configurations may present "defects", such as singly-occupied or empty nearest-neighbor sites. The energetic cost of the different defects depend on the strength of the couplings V and U, and in this way one of them may prevail over the others depending on the ratio V/U. Specifically, the different CDW ground states and their corresponding defects are shown below:

•$U \gtrsim V \gtrsim U/2$ (singly occupied nearest-neighbor defects): The degenerate ground states and energy are given by,

$$\begin{aligned} |gs\rangle_\ell &= |CDW^{[20]}\rangle_\ell \otimes |11\rangle \otimes |CDW^{[02]}\rangle_{L-\ell-2}, \\ \frac{E_{gs}}{LU} &= \frac{1}{2} + \frac{1}{L}(v-1), \end{aligned} \tag{4.11}$$

where

$$|CDW^{[20]}\rangle_\ell = \otimes_{k=1}^{\ell/2} |20\rangle, \tag{4.12}$$

$$|CDW^{[02]}\rangle_\ell = \otimes_{k=1}^{\ell/2} |02\rangle \tag{4.13}$$

with $\ell = 0, 2, 4, ..., L$ indicating the sizes of the two possible charge-density-wave configurations in the degenerate subspace, $v = V/U$ and E_{gs} the ground state energy.

•$V \gtrsim U$ (empty nearest-neighbor defects): In this case the degenerate ground states and energy are given by,

$$\begin{aligned} |gs\rangle_\ell &= |CDW^{[20]}\rangle_\ell \otimes |CDW^{[02]}\rangle_{L-\ell}, \\ \frac{E_{gs}}{LU} &= \frac{1}{2}, \end{aligned} \tag{4.14}$$

with $\ell = 0, 2, ..., L$ indicating the defect position, i.e., the pair of empty $(\ell, \ell+1)$ nearest-neighbor sites.

Therefore, despite the system is always characterized by a macroscopic CDW phase for both cases, at a few-body level the wavefunction has different properties. Considering a nonzero small hopping in the system $t \sim \epsilon$ shall not change significantly this picture, leading only to second-order perturbative corrections to the wavefunction. We conclude in this way that the entanglement gap minima observed in Fig.18 along these couplings are a consequence of the different types of few-body defects in the ground state wavefunction. We also remark that along this line the closure of entanglement gap follows between singlet eigenvalues (not shown), a different phenomenology as compared to the triplet-singlet superconducting phase transition discussed in the previous section.

Case $U, V < 0$ (attractive): The analysis of the attractive case follows similarly to the previous one. The different defects and fluctuations, however, appear in the ground state

from higher orders corrections in perturbation theory. Therefore, despite the entanglement gap may still capture these fluctuations are much weaker, in accordance with our numerical results, where the minimum observed in the quantifier is much smoother as compared to the repulsive case. Specifically, considering the infinite coupling limit the degenerate ground states are given by clusters of fully occupied sites, such as $|...022...220...\rangle$. Perturbative corrections correspond e.g. to hoppings of single fermions ($|20\rangle \rightarrow |11\rangle$) or doublons ($|20\rangle \rightarrow |02\rangle$) at the edges of the clusters. The prevalence of these two "defects" depend on the ratio V/U, thus leading to different few-body quantum fluctuations in the wavefunction.

4.3 Conclusions

In this work we studied the ground state properties of the one-dimensional extended Hubbard model, composed of half-spin fermions, from the perspective of its *particle* reduced density matrices. Focusing in the case of two-fermion reduced density matrices, we studied different facets of the quantum correlations and coherence on such states borrowing tools from Quantum Information and Entanglement theories. Specifically, we analysed (i) the entanglement entropy of the reduced states, corresponding to the entanglement between 2 fermions with the rest of $N-2$ fermions in the system; (ii) the irreducible two-body correlations contained in the cumulant matrix; (iii) quantum coherences obtained from the off-diagonal elements of the reduced density matrix elements and (iv) the spectral structure and gap of the reduced density matrix.

In a general form, we obtained that all of the above quantifiers provide a qualitative view of the phase diagram of the model, showing peculiar behaviors such as discontinuities, maximum or minimum values at the quantum phase transitions and are complementary to each other for a better description of the system properties. Interestingly, performing a finite-size scaling analysis of the quantifiers around the BOW related phase transitions, i.e., for a fixed $U/t = 4$ and varying V/t for different system sizes, we found that while the entanglement of particles Q_2, the coherence C_2 and the entanglement gap Ω_2 have their maximum/minimum at the critical value $V^* \approx 2.22$ in the thermodynamic limit, the irreducible correlations D_2 have critical value closer to $V^* \approx 2.02$. Comparing these results with the literature we tend to conclude that while Q_2, C_2 and Ω_2 are most sensitive to the BOW-CDW phase transition, D_2 on the other hand is most related to the SDW-BOW phase transition.

We observed (numerically) that the two-fermion reduced density matrix has a $su(2)$ symmetry, thus splitting the Hilbert space into singlet and triplet subspaces. The overlap of the reduced matrix on such subspaces is intriguingly constant along all phase diagram, depending only on the number of sites L in the system. In the thermodynamic limit the overlap onto all subspaces tend to be equal.

These symmetries opened interesting avenues for the investigation of the spectral properties of the reduced state. Focusing our analysis on the superconducting region of the phase diagram, we first observed that the dominant (largest) eigenvalues of the reduced matrix on the different subspaces cross at a critical interacting strength $U^*_{ss-ts}(L, V/t)$. Thus the dominant eigenvalue of the reduced state shifts from the singlet subspace to the triplet one, signaling different dominant pairing orderings for the fermionic particles. Moreover, studying the structure of the dominant eigenvector, we showed that the dominance of a singlet or triplet eigenvalue in the spectrum of the reduced density matrix is related to the spatial distance between the fermionic pairs on the eigenvectors. Precisely, within the singlet subspace the fermion pairs tend to be spatially closer to each other when the singlet eigenvalue is dominant in the full spectrum. As one moves towards the TS phase these singlet pairs tend to move apart from each other, as well as decreasing the corresponding singlet eigenvalue. The same mechanism occurs for the triplet pairs and their eigenvalues.

An interesting perspective for our work stands on delineating possible connections between our quantifiers with other approaches with more direct experimental access, such as optical conductivity and optical gap studies [75, 111]. These could be experimentally probed by spectroscopy approaches, and similarly to our quantifiers they are also based on two-particle correlations. Nevertheless, a direct relation among them is not straightforward and would require a deeper analysis.

Referências

[1] FISHMAN, M.; WHITE, S.; STOUDENMIRE, E. M. The ITensor Software Library for Tensor Network Calculations. SciPost Physics Codebases, p. 004, ago. 2022. ISSN 2949-804X. Disponível em: <https://scipost.org/10.21468/SciPostPhysCodeb.4>. Citado na página 5.

[2] FISHMAN, M.; WHITE, S.; STOUDENMIRE, E. M. Codebase release 0.3 for ITensor. SciPost Physics Codebases, p. 004, ago. 2022. ISSN 2949-804X. Disponível em: <https://scipost.org/SciPostPhysCodeb.4-r0.3>. Citado na página 5.

[3] FERREIRA, D. L. B. itensor-hubbardmodel-2particle: Código para tese. 2023. `https://github.com/diegobragaferreira/itensor-hubbardmodel-2particle`. Citado na página 5.

[4] FRASER, G. (Ed.). The New Physics: For the Twenty-First Century. Cambridge: Cambridge University Press, 2006. Disponível em: <https://www.cambridge.org/core/books/new-physics/DC742EA777D1202C50EE6B2A2A5D5581>. Citado na página 10.

[5] WEN, X.-G. Topological Order: From Long-Range Entangled Quantum Matter to a Unified Origin of Light and Electrons. International Scholarly Research Notices, v. 2013, n. 1, p. 198710, 2013. ISSN 2356-7872. _eprint: https://onlinelibrary.wiley.com/doi/pdf/10.1155/2013/198710. Disponível em: <https://onlinelibrary.wiley.com/doi/abs/10.1155/2013/198710>. Citado na página 10.

[6] AMICO, L. et al. Entanglement in many-body systems. Reviews of Modern Physics, v. 80, n. 2, p. 517–576, maio 2008. Publisher: American Physical Society. Disponível em: <https://link.aps.org/doi/10.1103/RevModPhys.80.517>. Citado 2 vezes nas páginas 10 e 11.

[7] ZENG, B. et al. Quantum Information Meets Quantum Matter: From Quantum Entanglement to Topological Phases of Many-Body Systems. New York, NY: Springer, 2019. (Quantum Science and Technology). ISBN 978-1-4939-9082-5 978-1-4939-9084-9. Disponível em: <http://link.springer.com/10.1007/978-1-4939-9084-9>. Citado na página 10.

[8] LI, H.; HALDANE, F. D. M. Entanglement Spectrum as a Generalization of Entanglement Entropy: Identification of Topological Order in Non-Abelian Fractional Quantum Hall Effect States. Physical Review Letters, v. 101, n. 1,

p. 010504, jul. 2008. Publisher: American Physical Society. Disponível em: <https://link.aps.org/doi/10.1103/PhysRevLett.101.010504>. Citado 2 vezes nas páginas 11 e 17.

[9] FIDKOWSKI, L. Entanglement Spectrum of Topological Insulators and Superconductors. Physical Review Letters, v. 104, n. 13, p. 130502, abr. 2010. Publisher: American Physical Society. Disponível em: <https://link.aps.org/doi/10.1103/PhysRevLett.104.130502>. Citado 2 vezes nas páginas 11 e 17.

[10] TURNER, A. M.; POLLMANN, F.; BERG, E. Topological phases of one-dimensional fermions: An entanglement point of view. Physical Review B, v. 83, n. 7, p. 075102, fev. 2011. Publisher: American Physical Society. Disponível em: <https://link.aps.org/doi/10.1103/PhysRevB.83.075102>. Citado 2 vezes nas páginas 11 e 17.

[11] MODI, K. et al. The classical-quantum boundary for correlations: Discord and related measures. Reviews of Modern Physics, v. 84, n. 4, p. 1655–1707, nov. 2012. Publisher: American Physical Society. Disponível em: <https://link.aps.org/doi/10.1103/RevModPhys.84.1655>. Citado na página 11.

[12] HORODECKI, R. et al. Quantum entanglement. Reviews of Modern Physics, v. 81, n. 2, p. 865–942, jun. 2009. Publisher: American Physical Society. Disponível em: <https://link.aps.org/doi/10.1103/RevModPhys.81.865>. Citado na página 11.

[13] STRELTSOV, A.; ADESSO, G.; PLENIO, M. B. Colloquium: Quantum coherence as a resource. Reviews of Modern Physics, v. 89, n. 4, p. 041003, out. 2017. Publisher: American Physical Society. Disponível em: <https://link.aps.org/doi/10.1103/RevModPhys.89.041003>. Citado na página 11.

[14] LOURENçO, A. C. et al. Genuine multipartite correlations distribution in the criticality of the Lipkin-Meshkov-Glick model. Physical Review B, v. 101, n. 5, p. 054431, fev. 2020. Publisher: American Physical Society. Disponível em: <https://link.aps.org/doi/10.1103/PhysRevB.101.054431>. Citado na página 11.

[15] OLIVEIRA, T. R. de; RIGOLIN, G.; OLIVEIRA, M. C. de. Genuine multipartite entanglement in quantum phase transitions. Physical Review A, v. 73, n. 1, p. 010305, jan. 2006. Publisher: American Physical Society. Disponível em: <https://link.aps.org/doi/10.1103/PhysRevA.73.010305>. Citado na página 11.

[16] HOFMANN, M.; OSTERLOH, A.; GüHNE, O. Scaling of genuine multiparticle entanglement close to a quantum phase transition. Physical Review B, v. 89, n. 13, p. 134101, abr. 2014. Publisher: American Physical Society. Disponível em: <https://link.aps.org/doi/10.1103/PhysRevB.89.134101>. Citado na página 11.

[17] KRUTITSKY, K. V.; OSTERLOH, A.; SCHüTZHOLD, R. Avalanche of entanglement and correlations at quantum phase transitions. Scientific Reports, v. 7, n. 1, p. 3634, jun. 2017. ISSN 2045-2322. Publisher: Nature Publishing Group. Disponível em: <https://www.nature.com/articles/s41598-017-03402-8>. Citado na página 11.

[18] BEGGI, A.; BUSCEMI, F.; BORDONE, P. Quantum correlations of identical particles subject to classical environmental noise. Quantum Information Processing, v. 15, n. 9, p. 3711–3743, set. 2016. ISSN 1573-1332. Disponível em: <https://doi.org/10.1007/s11128-016-1334-8>. Citado na página 11.

[19] OSTERLOH, A. et al. Scaling of entanglement close to a quantum phase transition. Nature, v. 416, n. 6881, p. 608–610, abr. 2002. ISSN 1476-4687. Publisher: Nature Publishing Group. Disponível em: <https://www.nature.com/articles/416608a>. Citado na página 11.

[20] IEMINI, F. et al. Signatures of many-body localization in the dynamics of two-site entanglement. Physical Review B, v. 94, n. 21, p. 214206, dez. 2016. Publisher: American Physical Society. Disponível em: <https://link.aps.org/doi/10.1103/PhysRevB.94.214206>. Citado na página 11.

[21] CAMPBELL, S.; POWER, M. J. M.; CHIARA, G. D. Dynamics and asymptotics of correlations in a many-body localized system. The European Physical Journal D, v. 71, n. 8, p. 206, ago. 2017. ISSN 1434-6079. Disponível em: <https://doi.org/10.1140/epjd/e2017-80302-8>. Citado na página 11.

[22] LIMA, L. S. Quantum correlation and entanglement in the Heisenberg model with biquadratic interaction on square lattice. The European Physical Journal D, v. 75, n. 1, p. 28, jan. 2021. ISSN 1434-6079. Disponível em: <https://doi.org/10.1140/epjd/s10053-021-00044-4>. Citado na página 11.

[23] IEMINI, F.; MACIEL, T. O.; VIANNA, R. O. Entanglement of indistinguishable particles as a probe for quantum phase transitions in the extended Hubbard model. Physical Review B, v. 92, n. 7, p. 075423, ago. 2015. Publisher: American Physical Society. Disponível em: <https://link.aps.org/doi/10.1103/PhysRevB.92.075423>. Citado na página 11.

[24] ALEXANDRADINATA, A.; HUGHES, T. L.; BERNEVIG, B. A. Trace index and spectral flow in the entanglement spectrum of topological insulators. Physical Review B, v. 84, n. 19, p. 195103, nov. 2011. Publisher: American Physical Society. Disponível em: <https://link.aps.org/doi/10.1103/PhysRevB.84.195103>. Citado 2 vezes nas páginas 11 e 17.

[25] BARGHATHI, H.; CASIANO-DIAZ, E.; MAESTRO, A. D. Particle partition entanglement of one dimensional spinless fermions. Journal of Statistical Mechanics: Theory and Experiment, v. 2017, n. 8, p. 083108, ago. 2017. ISSN 1742-5468. Publisher: IOP Publishing and SISSA. Disponível em: <https://doi.org/10.1088/1742-5468/aa819a>. Citado na página 11.

[26] HAQUE, M.; ZOZULYA, O. S.; SCHOUTENS, K. Entanglement between particle partitions in itinerant many-particle states. Journal of Physics A: Mathematical and Theoretical, v. 42, n. 50, p. 504012, dez. 2009. ISSN 1751-8121. Disponível em: <https://doi.org/10.1088/1751-8113/42/50/504012>. Citado 2 vezes nas páginas 11 e 17.

[27] HERDMAN, C. M.; MAESTRO, A. D. Particle partition entanglement of bosonic Luttinger liquids. Physical Review B, v. 91, n. 18, p. 184507, maio 2015. Publisher: American Physical Society. Disponível em: <https://link.aps.org/doi/10.1103/PhysRevB.91.184507>. Citado 2 vezes nas páginas 11 e 17.

[28] LIU, Z.; FAN, H. Particle entanglement in rotating gases. Physical Review A, v. 81, n. 6, p. 062302, jun. 2010. Publisher: American Physical Society. Disponível em: <https://link.aps.org/doi/10.1103/PhysRevA.81.062302>. Citado 2 vezes nas páginas 11 e 17.

[29] RAMMELMüLLER, L. et al. Evolution from few- to many-body physics in one-dimensional Fermi systems: One- and two-body density matrices and particle-partition entanglement. Physical Review A, v. 96, n. 3, p. 033635, set. 2017. Publisher: American Physical Society. Disponível em: <https://link.aps.org/doi/10.1103/PhysRevA.96.033635>. Citado na página 11.

[30] HAQUE, M.; ZOZULYA, O.; SCHOUTENS, K. Entanglement Entropy in Fermionic Laughlin States. Physical Review Letters, v. 98, n. 6, p. 060401, fev. 2007. Publisher: American Physical Society. Disponível em: <https://link.aps.org/doi/10.1103/PhysRevLett.98.060401>. Citado na página 11.

[31] TULLIO, M. D. et al. Fermionic entanglement in the Lipkin model. Physical Review A, v. 100, n. 6, p. 062104, dez. 2019. Publisher: American Physical Society. Disponível em: <https://link.aps.org/doi/10.1103/PhysRevA.100.062104>. Citado na página 11.

[32] MALVEZZI, A. L. et al. Quantum correlations and coherence in spin-1 Heisenberg chains. Physical Review B, v. 93, n. 18, p. 184428, maio 2016. Publisher: American Physical Society. Disponível em: <https://link.aps.org/doi/10.1103/PhysRevB.93.184428>. Citado na página 11.

[33] CHIARA, G. D.; SANPERA, A. Genuine quantum correlations in quantum many-body systems: a review of recent progress. Reports on Progress in Physics, v. 81, n. 7, p. 074002, jun. 2018. ISSN 0034-4885. Publisher: IOP Publishing. Disponível em: <https://doi.org/10.1088/1361-6633/aabf61>. Citado na página 11.

[34] HUBBARD, J. Electron correlations in narrow energy bands. Proceedings of the Royal Society of London. Series A. Mathematical and Physical Sciences, v. 276, n. 1365, p. 238–257, jan. 1997. Publisher: Royal Society. Disponível em: <https://royalsocietypublishing.org/doi/10.1098/rspa.1963.0204>. Citado 2 vezes nas páginas 11 e 12.

[35] FERREIRA, D. L. B. et al. Quantum correlations, entanglement spectrum, and coherence of the two-particle reduced density matrix in the extended hubbard model. Phys. Rev. B, American Physical Society, v. 105, p. 115145, Mar 2022. Disponível em: <https://link.aps.org/doi/10.1103/PhysRevB.105.115145>. Citado na página 11.

[36] GU, S.-J. et al. Entanglement and Quantum Phase Transition in the Extended Hubbard Model. Physical Review Letters, v. 93, n. 8, p. 086402, ago. 2004. Publisher: American Physical Society. Disponível em: <https://link.aps.org/doi/10.1103/PhysRevLett.93.086402>. Citado na página 11.

[37] DENG, S.-S.; GU, S.-J.; LIN, H.-Q. Block-block entanglement and quantum phase transitions in the one-dimensional extended Hubbard model. Physical Review B, v. 74, n. 4, p. 045103, jul. 2006. Publisher: American Physical Society. Disponível em: <https://link.aps.org/doi/10.1103/PhysRevB.74.045103>. Citado 2 vezes nas páginas 11 e 34.

[38] ZHEN, Y.; WEN-QIANG, N. Negativity in the Extended Hubbard Model under External Magnetic Field. Chinese Physics Letters, v. 25, n. 1, p. 31, jan. 2008. ISSN 0256-307X. Disponível em: <https://doi.org/10.1088/0256-307X/25/1/009>. Citado na página 11.

[39] MUND, C.; LEGEZA, ; NOACK, R. M. Quantum information analysis of the phase diagram of the half-filled extended Hubbard model. Physical Review B, v. 79, n. 24, p. 245130, jun. 2009. Publisher: American Physical Society. Disponível em: <https://link.aps.org/doi/10.1103/PhysRevB.79.245130>. Citado na página 11.

[40] Guang-Hua, Liu and Chun-Hai, Wang. Existence of Bond-Order-Wave Phase in One-Dimensional Extended Hubbard Model. Communications in Theoretical Physics, v. 55, n. 4, p. 702, abr. 2011. ISSN 0253-6102. Disponível em: <https://doi.org/10.1088/0253-6102/55/4/35>. Citado na página 11.

[41] GIGENA, N.; ROSSIGNOLI, R. Entanglement in fermion systems. Physical Review A, v. 92, n. 4, p. 042326, out. 2015. Publisher: American Physical Society. Disponível em: <https://link.aps.org/doi/10.1103/PhysRevA.92.042326>. Citado na página 11.

[42] BARBIERO, L.; FAZZINI, S.; MONTORSI, A. Non-local order parameters as a probe for phase transitions in the extended Fermi-Hubbard model. The European Physical Journal Special Topics, v. 226, n. 12, p. 2697–2704, jul. 2017. ISSN 1951-6401. Disponível em: <https://doi.org/10.1140/epjst/e2016-60386-1>. Citado na página 11.

[43] CHUNG, M.-H. Phase transitions in the one-dimensional ionic Hubbard model. Journal of the Korean Physical Society, v. 78, n. 8, p. 700–705, abr. 2021. ISSN 1976-8524. Disponível em: <https://doi.org/10.1007/s40042-021-00099-x>. Citado na página 11.

[44] RAUSCH, R.; PESCHKE, M. Topological phases arising from attractive interaction and pair hopping in the extended Hubbard model. New Journal of Physics, v. 22, n. 7, p. 073051, jul. 2020. ISSN 1367-2630. Publisher: IOP Publishing. Disponível em: <https://doi.org/10.1088/1367-2630/ab9c65>. Citado na página 11.

[45] PANDEY, B.; PATI, S. K. Triplet superfluidity on a triangular ladder with dipolar fermions. Physical Review B, v. 95, n. 8, p. 085105, fev. 2017. Publisher: American Physical Society. Disponível em: <https://link.aps.org/doi/10.1103/PhysRevB.95.085105>. Citado na página 11.

[46] IEMINI, F.; VIANNA, R. O. Computable measures for the entanglement of indistinguishable particles. Physical Review A, v. 87, n. 2, p. 022327, fev. 2013. Publisher: American Physical Society. Disponível em: <https://link.aps.org/doi/10.1103/PhysRevA.87.022327>. Citado 2 vezes nas páginas 11 e 16.

[47] IEMINI, F. et al. Quantifying quantum correlations in fermionic systems using witness operators. Quantum Information Processing, v. 12, n. 2, p. 733–746, fev. 2013. ISSN 1573-1332. Disponível em: <https://doi.org/10.1007/s11128-012-0415-6>. Citado 2 vezes nas páginas 11 e 16.

[48] IEMINI, F.; DEBARBA, T.; VIANNA, R. O. Quantumness of correlations in indistinguishable particles. Physical Review A, v. 89, n. 3, p. 032324, mar. 2014. Publisher: American Physical Society. Disponível em: <https://link.aps.org/doi/10.1103/PhysRevA.89.032324>. Citado 2 vezes nas páginas 11 e 16.

[49] BALACHANDRAN, A. P. et al. Entanglement and Particle Identity: A Unifying Approach. Physical Review Letters, v. 110, n. 8, p.

080503, fev. 2013. Publisher: American Physical Society. Disponível em: <https://link.aps.org/doi/10.1103/PhysRevLett.110.080503>. Citado 2 vezes nas páginas 11 e 16.

[50] BALACHANDRAN, A. P. et al. Algebraic approach to entanglement and entropy. Physical Review A, v. 88, n. 2, p. 022301, ago. 2013. Publisher: American Physical Society. Disponível em: <https://link.aps.org/doi/10.1103/PhysRevA.88.022301>. Citado 2 vezes nas páginas 11 e 16.

[51] GHIRARDI, G.; MARINATTO, L.; WEBER, T. Entanglement and Properties of Composite Quantum Systems: A Conceptual and Mathematical Analysis. Journal of Statistical Physics, v. 108, n. 1, p. 49–122, jul. 2002. ISSN 1572-9613. Disponível em: <https://doi.org/10.1023/A:1015439502289>. Citado 2 vezes nas páginas 11 e 16.

[52] GHIRARDI, G.; MARINATTO, L. General criterion for the entanglement of two indistinguishable particles. Physical Review A, v. 70, n. 1, p. 012109, jul. 2004. Publisher: American Physical Society. Disponível em: <https://link.aps.org/doi/10.1103/PhysRevA.70.012109>. Citado 2 vezes nas páginas 11 e 16.

[53] SCHLIEMANN, J. et al. Quantum correlations in two-fermion systems. Physical Review A, v. 64, n. 2, p. 022303, jul. 2001. Publisher: American Physical Society. Disponível em: <https://link.aps.org/doi/10.1103/PhysRevA.64.022303>. Citado 2 vezes nas páginas 11 e 16.

[54] SCHLIEMANN, J.; LOSS, D.; MACDONALD, A. H. Double-occupancy errors, adiabaticity, and entanglement of spin qubits in quantum dots. Physical Review B, v. 63, n. 8, p. 085311, fev. 2001. Publisher: American Physical Society. Disponível em: <https://link.aps.org/doi/10.1103/PhysRevB.63.085311>. Citado 2 vezes nas páginas 11 e 16.

[55] ECKERT, K. et al. Quantum Correlations in Systems of Indistinguishable Particles. Annals of Physics, v. 299, n. 1, p. 88–127, jul. 2002. ISSN 0003-4916. Disponível em: <https://www.sciencedirect.com/science/article/pii/S0003491602962688>. Citado 2 vezes nas páginas 11 e 16.

[56] LI, Y. S. et al. Entanglement in a two-identical-particle system. Physical Review A, v. 64, n. 5, p. 054302, out. 2001. Publisher: American Physical Society. Disponível em: <https://link.aps.org/doi/10.1103/PhysRevA.64.054302>. Citado 2 vezes nas páginas 11 e 16.

[57] BARNUM, H. et al. A Subsystem-Independent Generalization of Entanglement. Physical Review Letters, v. 92, n. 10, p. 107902, mar. 2004. Publisher: American Physical

Society. Disponível em: <https://link.aps.org/doi/10.1103/PhysRevLett.92.107902>. Citado 2 vezes nas páginas 11 e 16.

[58] SOMMA, R. et al. Nature and measure of entanglement in quantum phase transitions. Physical Review A, v. 70, n. 4, p. 042311, out. 2004. Publisher: American Physical Society. Disponível em: <https://link.aps.org/doi/10.1103/PhysRevA.70.042311>. Citado 2 vezes nas páginas 11 e 16.

[59] PAšKAUSKAS, R.; YOU, L. Quantum correlations in two-boson wave functions. Physical Review A, v. 64, n. 4, p. 042310, set. 2001. Publisher: American Physical Society. Disponível em: <https://link.aps.org/doi/10.1103/PhysRevA.64.042310>. Citado 2 vezes nas páginas 11 e 16.

[60] PLASTINO, A. R.; MANZANO, D.; DEHESA, J. S. Separability criteria and entanglement measures for pure states of N identical fermions. Europhysics Letters, v. 86, n. 2, p. 20005, maio 2009. ISSN 0295-5075. Disponível em: <https://doi.org/10.1209/0295-5075/86/20005>. Citado 2 vezes nas páginas 11 e 16.

[61] ZANDER, C.; PLASTINO, A. R. Uncertainty relations and entanglement in fermion systems. Physical Review A, v. 81, n. 6, p. 062128, jun. 2010. Publisher: American Physical Society. Disponível em: <https://link.aps.org/doi/10.1103/PhysRevA.81.062128>. Citado 2 vezes nas páginas 11 e 16.

[62] DEBARBA, T.; VIANNA, R. O.; IEMINI, F. Quantumness of correlations in fermionic systems. Physical Review A, v. 95, n. 2, p. 022325, fev. 2017. Publisher: American Physical Society. Disponível em: <https://link.aps.org/doi/10.1103/PhysRevA.95.022325>. Citado 2 vezes nas páginas 11 e 16.

[63] GIGENA, N.; ROSSIGNOLI, R. Bipartite entanglement in fermion systems. Physical Review A, v. 95, n. 6, p. 062320, jun. 2017. Publisher: American Physical Society. Disponível em: <https://link.aps.org/doi/10.1103/PhysRevA.95.062320>. Citado na página 11.

[64] TULLIO, M. D.; GIGENA, N.; ROSSIGNOLI, R. Fermionic entanglement in superconducting systems. Physical Review A, v. 97, n. 6, p. 062109, jun. 2018. Publisher: American Physical Society. Disponível em: <https://link.aps.org/doi/10.1103/PhysRevA.97.062109>. Citado na página 11.

[65] GIGENA, N.; TULLIO, M. D.; ROSSIGNOLI, R. One-body entanglement as a quantum resource in fermionic systems. Physical Review A, v. 102, n. 4, p. 042410, out. 2020. Publisher: American Physical Society. Disponível em: <https://link.aps.org/doi/10.1103/PhysRevA.102.042410>. Citado na página 11.

[66] BENATTI, F. et al. Entanglement in indistinguishable particle systems. Physics Reports, v. 878, p. 1–27, set. 2020. ISSN 0370-1573. Disponível em: <https://www.sciencedirect.com/science/article/pii/S0370157320302520>. Citado na página 11.

[67] BENAVOLI, A.; FACCHINI, A.; ZAFFALON, M. Quantum Indistinguishability through Exchangeable Desirable Gambles. In: Proceedings of the Twelveth International Symposium on Imprecise Probability: Theories and Applications. PMLR, 2021. p. 22–31. ISSN: 2640-3498. Disponível em: <https://proceedings.mlr.press/v147/benavoli21a.html>. Citado na página 11.

[68] GIGENA, N.; TULLIO, M. D.; ROSSIGNOLI, R. Many-body entanglement in fermion systems. Physical Review A, v. 103, n. 5, p. 052424, maio 2021. Publisher: American Physical Society. Disponível em: <https://link.aps.org/doi/10.1103/PhysRevA.103.052424>. Citado na página 11.

[69] SóLYOM, J. The Fermi gas model of one-dimensional conductors. Advances in Physics, v. 28, n. 2, p. 201–303, abr. 1979. ISSN 0001-8732. Publisher: Taylor & Francis _eprint: https://doi.org/10.1080/00018737900101375. Disponível em: <https://doi.org/10.1080/00018737900101375>. Citado na página 12.

[70] LIN, H. Q.; CAMPBELL, D. K.; CLAY, R. T. Broken symmetries in the one-dimensional extended hubbard model. Chinese Journal of Physics, v. 38, n. 1, p. 1–11, 2000. Disponível em: `https://arxiv.org/abs/cond-mat/9903366`. Citado 4 vezes nas páginas 13, 14, 34 e 37.

[71] NAKAMURA, M. Tricritical behavior in the extended Hubbard chains. Physical Review B, v. 61, n. 24, p. 16377–16392, jun. 2000. Publisher: American Physical Society. Disponível em: <https://link.aps.org/doi/10.1103/PhysRevB.61.16377>. Citado 3 vezes nas páginas 13, 14 e 37.

[72] SENGUPTA, P.; SANDVIK, A. W.; CAMPBELL, D. K. Bond-order-wave phase and quantum phase transitions in the one-dimensional extended Hubbard model. Physical Review B, v. 65, n. 15, p. 155113, abr. 2002. Publisher: American Physical Society. Disponível em: <https://link.aps.org/doi/10.1103/PhysRevB.65.155113>. Citado 3 vezes nas páginas 13, 14 e 35.

[73] ZHANG, Y. Z. Dimerization in a Half-Filled One-Dimensional Extended Hubbard Model. Physical Review Letters, v. 92, n. 24, p. 246404, jun. 2004. Publisher: American Physical Society. Disponível em: <https://link.aps.org/doi/10.1103/PhysRevLett.92.246404>. Citado 3 vezes nas páginas 13, 14 e 35.

[74] DALMONTE, M. et al. Gap scaling at Berezinskii-Kosterlitz-Thouless quantum critical points in one-dimensional Hubbard and Heisenberg models. Physical Review B, v. 91, n. 16, p. 165136, abr. 2015. Publisher: American Physical Society. Disponível em: <https://link.aps.org/doi/10.1103/PhysRevB.91.165136>. Citado 3 vezes nas páginas 13, 14 e 35.

[75] JECKELMANN, E. Ground-State Phase Diagram of a Half-Filled One-Dimensional Extended Hubbard Model. Physical Review Letters, v. 89, n. 23, p. 236401, nov. 2002. Publisher: American Physical Society. Disponível em: <https://link.aps.org/doi/10.1103/PhysRevLett.89.236401>. Citado 4 vezes nas páginas 13, 14, 35 e 45.

[76] EJIMA, S.; NISHIMOTO, S. Phase Diagram of the One-Dimensional Half-Filled Extended Hubbard Model. Physical Review Letters, v. 99, n. 21, p. 216403, nov. 2007. Publisher: American Physical Society. Disponível em: <https://link.aps.org/doi/10.1103/PhysRevLett.99.216403>. Citado 3 vezes nas páginas 13, 14 e 35.

[77] SANDVIK, A. W.; BALENTS, L.; CAMPBELL, D. K. Ground State Phases of the Half-Filled One-Dimensional Extended Hubbard Model. Physical Review Letters, v. 92, n. 23, p. 236401, jun. 2004. Publisher: American Physical Society. Disponível em: <https://link.aps.org/doi/10.1103/PhysRevLett.92.236401>. Citado 3 vezes nas páginas 13, 14 e 35.

[78] SHINJO, K. et al. Machine Learning Phase Diagram in the Half-filled One-dimensional Extended Hubbard Model. Journal of the Physical Society of Japan, v. 88, n. 6, p. 065001, jun. 2019. ISSN 0031-9015. Publisher: The Physical Society of Japan. Disponível em: <https://journals.jps.jp/doi/10.7566/JPSJ.88.065001>. Citado 2 vezes nas páginas 13 e 37.

[79] SHINJO, K. et al. Characterization of photoexcited states in the half-filled one-dimensional extended Hubbard model assisted by machine learning. Physical Review B, v. 101, n. 19, p. 195136, maio 2020. Publisher: American Physical Society. Disponível em: <https://link.aps.org/doi/10.1103/PhysRevB.101.195136>. Citado 2 vezes nas páginas 13 e 37.

[80] QU, D.-W. et al. Spin-triplet pairing induced by near-neighbor attraction in the extended Hubbard model for cuprate chain. Communications Physics, v. 5, n. 1, p. 257, out. 2022. ISSN 2399-3650. Publisher: Nature Publishing Group. Disponível em: <https://www.nature.com/articles/s42005-022-01030-x>. Citado na página 13.

[81] KUBO, R. Generalized Cumulant Expansion Method. Journal of the Physical Society of Japan, v. 17, n. 7, p. 1100–1120, jul. 1962. ISSN 0031-9015. Publisher: The Physical

Society of Japan. Disponível em: <https://journals.jps.jp/doi/10.1143/JPSJ.17.1100>. Citado na página 16.

[82] PLASTINO, A. R.; MANZANO, D.; DEHESA, J. S. Separability criteria and entanglement measures for pure states of N identical fermions. Europhysics Letters, v. 86, n. 2, p. 20005, maio 2009. ISSN 0295-5075. Disponível em: <https://doi.org/10.1209/0295-5075/86/20005>. Citado na página 17.

[83] MAJTEY, A. P. et al. Multipartite concurrence for identical-fermion systems. Physical Review A, v. 93, n. 3, p. 032335, mar. 2016. Publisher: American Physical Society. Disponível em: <https://link.aps.org/doi/10.1103/PhysRevA.93.032335>. Citado na página 17.

[84] BAUMGRATZ, T.; CRAMER, M.; PLENIO, M. B. Quantifying Coherence. Physical Review Letters, v. 113, n. 14, p. 140401, set. 2014. Publisher: American Physical Society. Disponível em: <https://link.aps.org/doi/10.1103/PhysRevLett.113.140401>. Citado na página 17.

[85] LUNDGREN, R. et al. Momentum-Space Entanglement Spectrum of Bosons and Fermions with Interactions. Physical Review Letters, v. 113, n. 25, p. 256404, dez. 2014. Publisher: American Physical Society. Disponível em: <https://link.aps.org/doi/10.1103/PhysRevLett.113.256404>. Citado na página 17.

[86] STERDYNIAK, A.; REGNAULT, N.; BERNEVIG, B. A. Extracting Excitations from Model State Entanglement. Physical Review Letters, v. 106, n. 10, p. 100405, mar. 2011. Publisher: American Physical Society. Disponível em: <https://link.aps.org/doi/10.1103/PhysRevLett.106.100405>. Citado na página 17.

[87] KUTZELNIGG, W.; MUKHERJEE, D. Cumulant expansion of the reduced density matrices. The Journal of Chemical Physics, v. 110, n. 6, p. 2800–2809, fev. 1999. ISSN 0021-9606. Disponível em: <https://doi.org/10.1063/1.478189>. Citado na página 18.

[88] BOUSSO, R. The holographic principle. Rev. Mod. Phys., v. 74, p. 825–874, 2002. Citado na página 21.

[89] MALDACENA, J. The Large-N Limit of Superconformal Field Theories and Supergravity. International Journal of Theoretical Physics, v. 38, n. 4, p. 1113–1133, abr. 1999. ISSN 1572-9575. Disponível em: <https://doi.org/10.1023/A:1026654312961>. Citado na página 21.

[90] GUBSER, S. S.; KLEBANOV, I. R.; POLYAKOV, A. M. Gauge theory correlators from non-critical string theory. Physics Letters B, v. 428, n. 1, p. 105–114, maio 1998. ISSN 0370-2693. Disponível em:

<https://www.sciencedirect.com/science/article/pii/S0370269398003773>. Citado na página 21.

[91] WITTEN, E. Anti de Sitter space and holography. Advances in Theoretical and Mathematical Physics, v. 2, n. 2, p. 253–291, jan. 1998. ISSN 1095-0753. Publisher: International Press of Boston. Disponível em: <https://link.intlpress.com/JDetail/1805563386639360001>. Citado na página 21.

[92] RYU, S.; TAKAYANAGI, T. Holographic Derivation of Entanglement Entropy from the anti–de Sitter Space/Conformal Field Theory Correspondence. Physical Review Letters, v. 96, n. 18, p. 181602, maio 2006. Publisher: American Physical Society. Disponível em: <https://link.aps.org/doi/10.1103/PhysRevLett.96.181602>. Citado na página 21.

[93] SWINGLE, B. Entanglement renormalization and holography. Physical Review D, v. 86, n. 6, p. 065007, set. 2012. Publisher: American Physical Society. Disponível em: <https://link.aps.org/doi/10.1103/PhysRevD.86.065007>. Citado na página 21.

[94] EVENBLY, G.; VIDAL, G. Tensor Network States and Geometry. Journal of Statistical Physics, v. 145, n. 4, p. 891–918, nov. 2011. ISSN 1572-9613. Disponível em: <https://doi.org/10.1007/s10955-011-0237-4>. Citado na página 21.

[95] VERSTRAETE, F.; PORRAS, D.; CIRAC, J. I. Density Matrix Renormalization Group and Periodic Boundary Conditions: A Quantum Information Perspective. Physical Review Letters, v. 93, n. 22, p. 227205, nov. 2004. Publisher: American Physical Society. Disponível em: <https://link.aps.org/doi/10.1103/PhysRevLett.93.227205>. Citado na página 21.

[96] FANNES, M.; NACHTERGAELE, B.; WERNER, R. F. Finitely correlated states on quantum spin chains. Communications in Mathematical Physics, v. 144, n. 3, p. 443–490, mar. 1992. ISSN 1432-0916. Disponível em: <https://doi.org/10.1007/BF02099178>. Citado na página 21.

[97] KLÜMPER, A.; SCHADSCHNEIDER, A.; ZITTARTZ, J. Matrix product ground states for one-dimensional spin-1 quantum antiferromagnets. EPL (Europhysics Letters), v. 24, n. 4, p. 293, 1993. Citado na página 21.

[98] VERSTRAETE, F.; CIRAC, J. I. Renormalization algorithms for Quantum-Many Body Systems in two and higher dimensions. arXiv, 2004. ArXiv:cond-mat/0407066. Disponível em: <http://arxiv.org/abs/cond-mat/0407066>. Citado na página 21.

[99] VIDAL, G. Class of Quantum Many-Body States That Can Be Efficiently Simulated. Physical Review Letters, v. 101, n. 11, p. 110501, set. 2008. Publisher: American Physical

Society. Disponível em: <https://link.aps.org/doi/10.1103/PhysRevLett.101.110501>. Citado na página 21.

[100] VIDAL, G. Entanglement Renormalization. Physical Review Letters, v. 99, n. 22, p. 220405, nov. 2007. Publisher: American Physical Society. Disponível em: <https://link.aps.org/doi/10.1103/PhysRevLett.99.220405>. Citado na página 21.

[101] ORúS, R. A practical introduction to tensor networks: Matrix product states and projected entangled pair states. Annals of Physics, v. 349, p. 117–158, out. 2014. ISSN 0003-4916. Disponível em: <https://www.sciencedirect.com/science/article/pii/S0003491614001596>. Citado na página 21.

[102] BRIDGEMAN, J. C.; CHUBB, C. T. Hand-waving and interpretive dance: an introductory course on tensor networks. Journal of Physics A: Mathematical and Theoretical, v. 50, n. 22, p. 223001, maio 2017. ISSN 1751-8121. Publisher: IOP Publishing. Disponível em: <https://doi.org/10.1088/1751-8121/aa6dc3>. Citado na página 21.

[103] VERSTRAETE, F.; MURG, V.; CIRAC, J. Matrix product states, projected entangled pair states, and variational renormalization group methods for quantum spin systems. Advances in Physics, v. 57, n. 2, p. 143–224, mar. 2008. ISSN 0001-8732. Publisher: Taylor & Francis _eprint: https://doi.org/10.1080/14789940801912366. Disponível em: <https://doi.org/10.1080/14789940801912366>. Citado na página 21.

[104] BIAMONTE, J.; BERGHOLM, V.; LANZAGORTA, M. Tensor network methods for invariant theory. Journal of Physics A: Mathematical and Theoretical, v. 46, n. 47, p. 475301, nov. 2013. ISSN 1751-8121. Publisher: IOP Publishing. Disponível em: <https://doi.org/10.1088/1751-8113/46/47/475301>. Citado na página 21.

[105] CIRAC, J. I.; VERSTRAETE, F. Renormalization and tensor product states in spin chains and lattices. Journal of Physics A: Mathematical and Theoretical, v. 42, n. 50, p. 504004, dez. 2009. ISSN 1751-8121. Disponível em: <https://doi.org/10.1088/1751-8113/42/50/504004>. Citado na página 21.

[106] PENROSE, R. The Road to Reality: A Complete Guide to the Laws of the Universe. London: Jonathan Cape, 2004. ISBN 978-0224044479. Citado na página 21.

[107] NIELSEN, M. A. The Fermionic canonical commutation relations and the Jordan-Wigner transform. 2005. Notas de aula. Disponível em: `http://michaelnielsen.org/blog/archive/notes/fermions.pdf`. Citado na página 30.

[108] SHI, Y. Entanglement of identical particles. Physics Letters A, v. 309, n. 3-4, p. 254–261, 2003. Citado na página 34.

[109] ŁYDżBA, P.; SOWIńSKI, T. Unconventional pairing in one-dimensional systems of a few mass-imbalanced ultracold fermions. Physical Review A, v. 101, n. 3, p. 033603, mar. 2020. Publisher: American Physical Society. Disponível em: <https://link.aps.org/doi/10.1103/PhysRevA.101.033603>. Citado na página 34.

[110] ESSLER, F. H. L. et al. The One-Dimensional Hubbard Model. [S.l.]: Cambridge University Press, 2005. Citado na página 35.

[111] KANCHARLA, G. S.; JECKELMANN, E. Optical conductivity of the one-dimensional extended hubbard model. Phys. Rev. B, v. 64, p. 235118, 2001. Citado na página 45.